CMEs and Transients

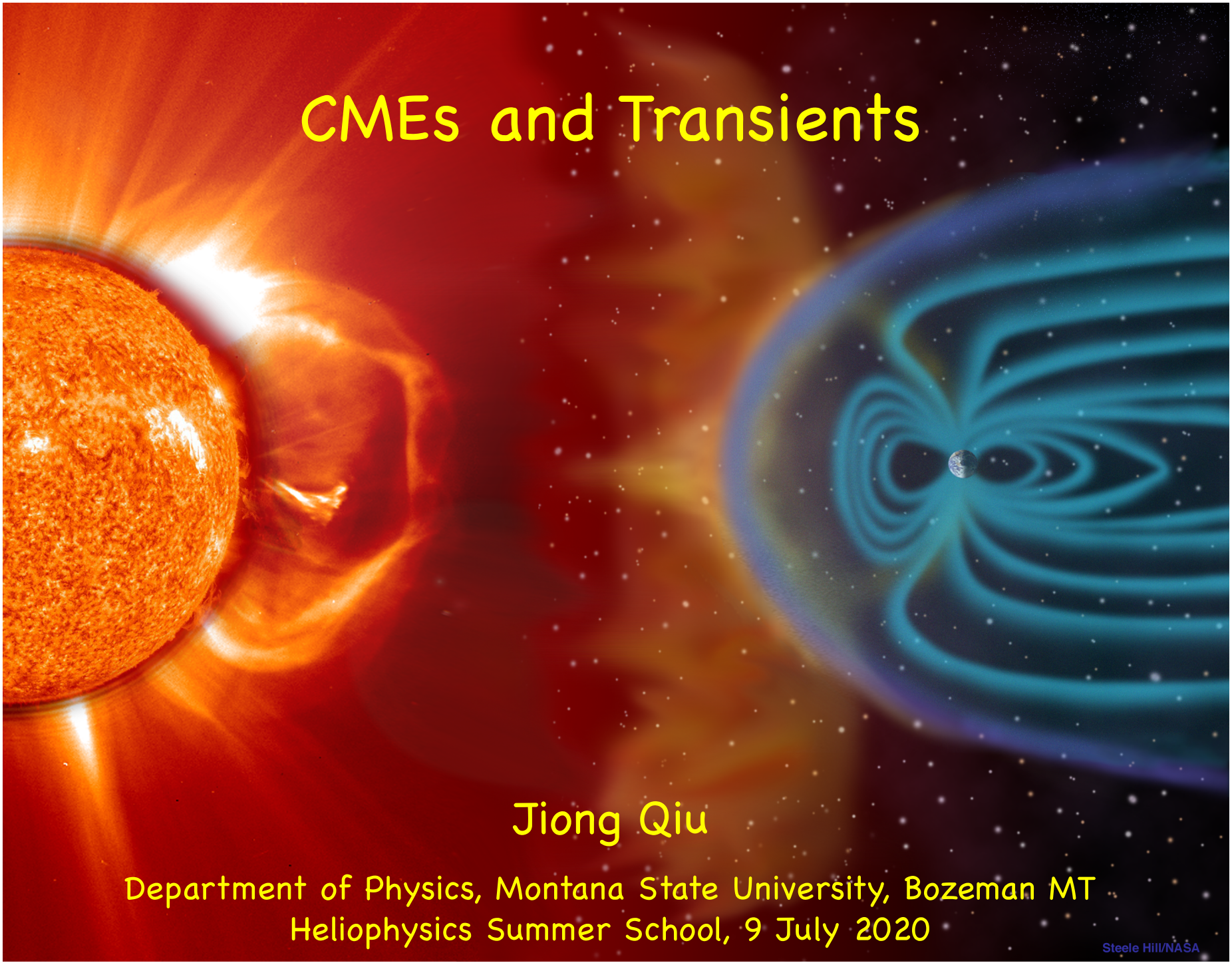

Jiong Qiu

Department of Physics, Montana State University, Bozeman MT

Heliophysics Summer School, 9 July 2020

Steele Hill/NASA

Outlines

- CMEs are among the most energetic events in the heliosphere, and have been observed and measured by generations of coronagraphs and other instruments.
- The typical three-part plasma structure of a white-light CME is often interpreted as representative of a magnetic flux rope, and its properties are studied from in-situ measurements of ICMEs.
- Unravelling mechanisms generating and accelerating CMEs in the solar corona helps predict space weather.

Energy release on the Sun in a day

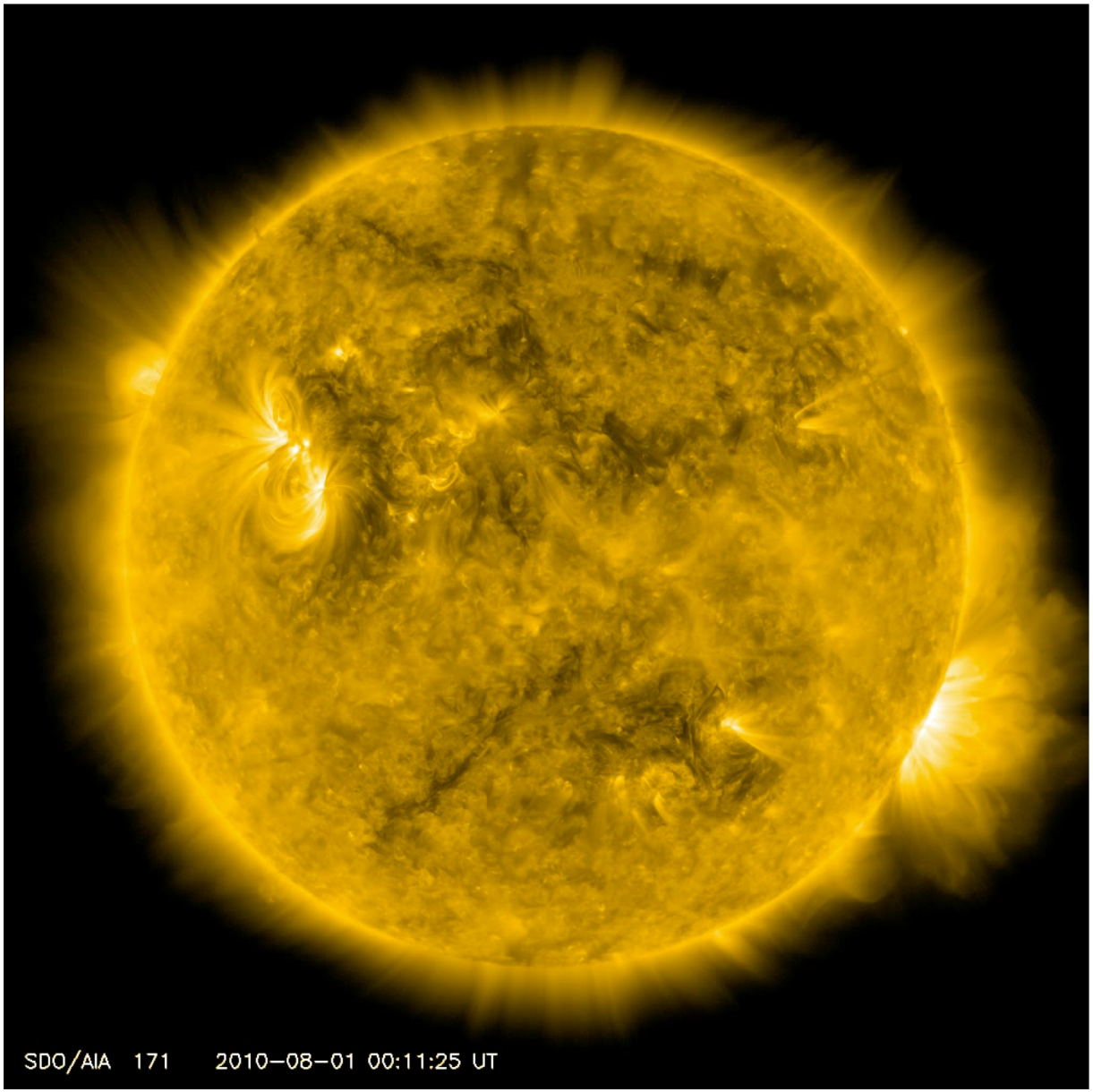

A perfect solar eruption on 2017-09-10

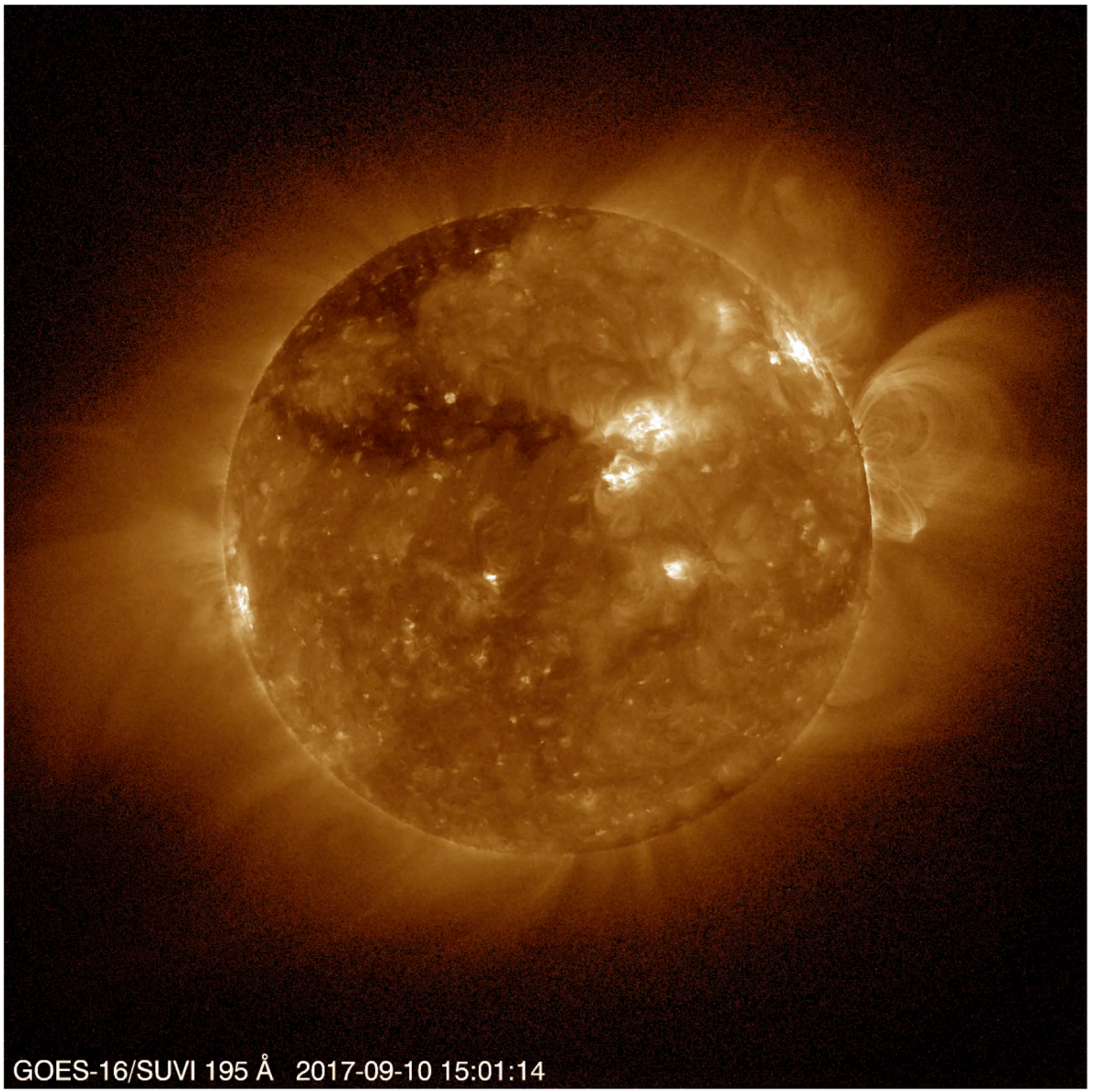

(Seaton & Darnel 2018)

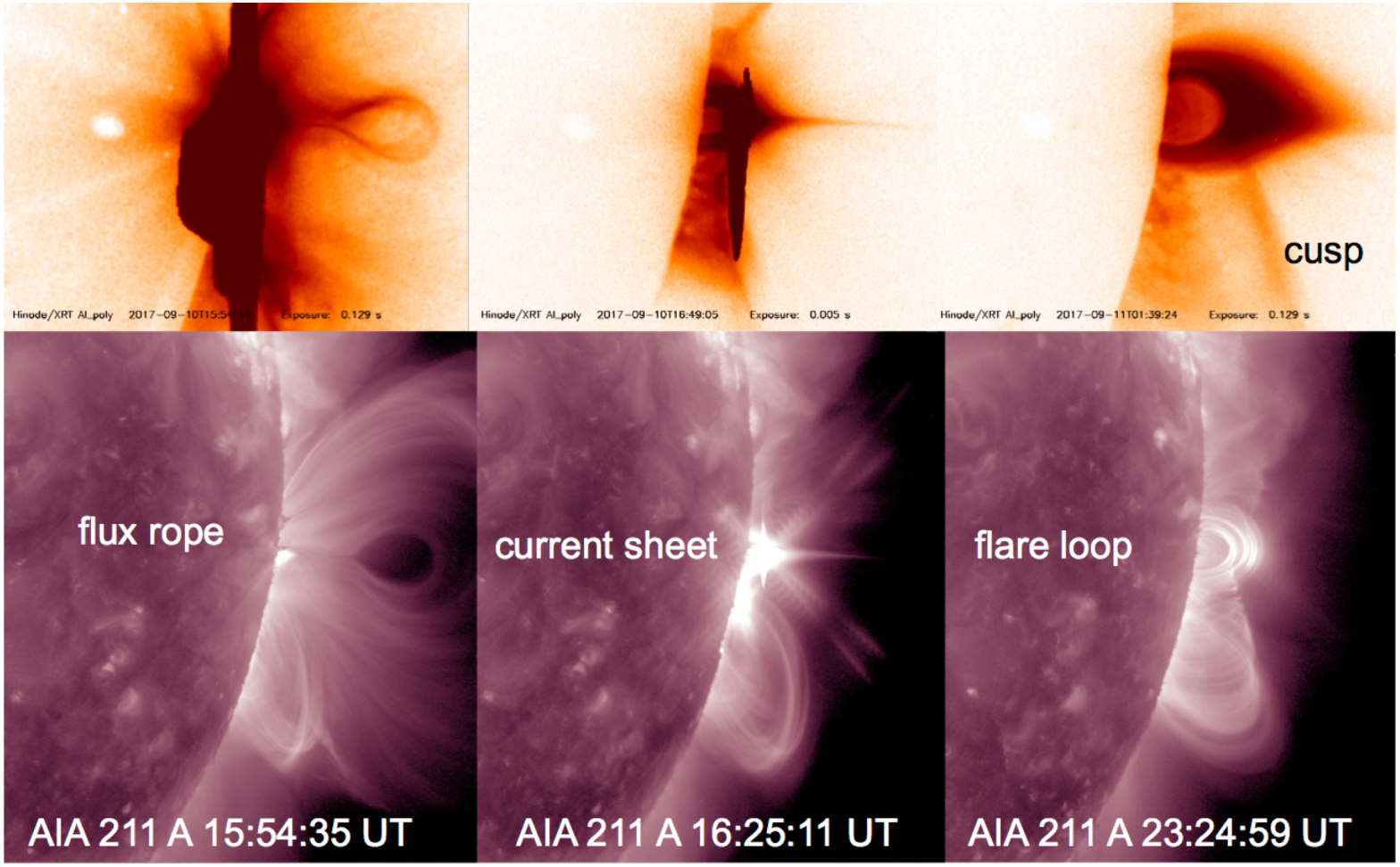
Hinode/XRT Al_poly 2017-09-10T15:54:14 Exposure: 0.129 s
Hinode/XRT Al_poly 2017-09-10T16:49:05 Exposure: 0.005 s
Hinode/XRT Al_poly 2017-09-11T01:39:24 Exposure: 0.129 s
cusp
flux rope
current sheet
flare loop
AIA 211 A 15:54:35 UT
AIA 211 A 16:25:11 UT
AIA 211 A 23:24:59 UT

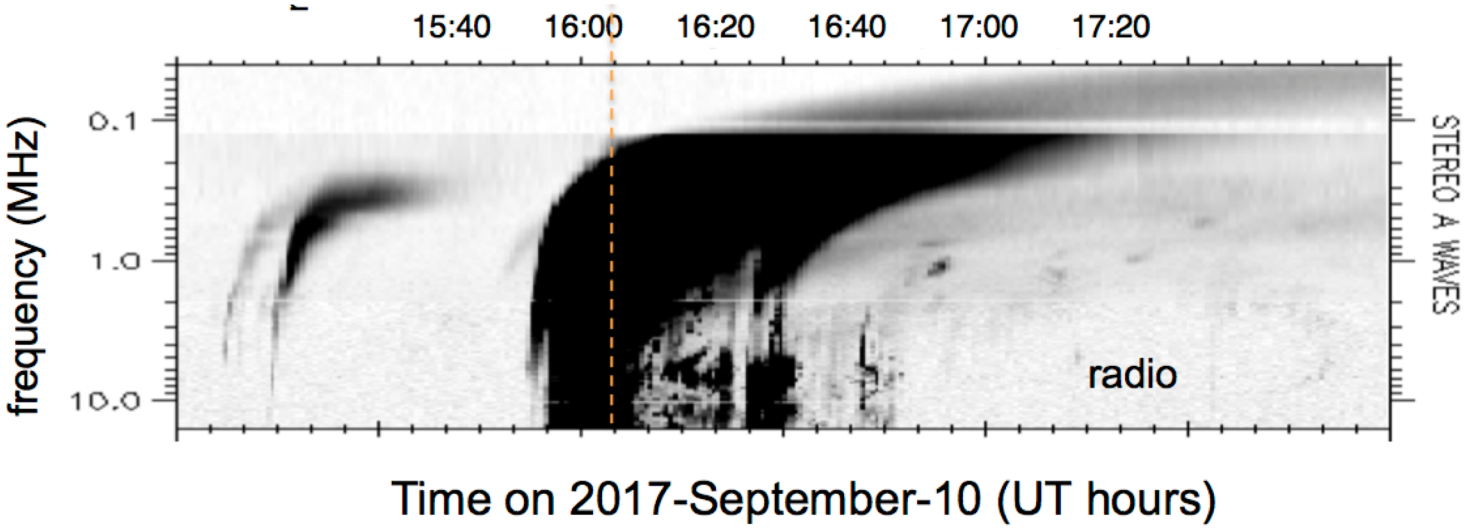
15:40
16:00
16:20
16:40
17:00
17:20
0.1
1.0
10.0
frequency (MHz)
STEREO A WAVES
radio
Time on 2017-September-10 (UT hours)

CMEs best seen by coronagraphs

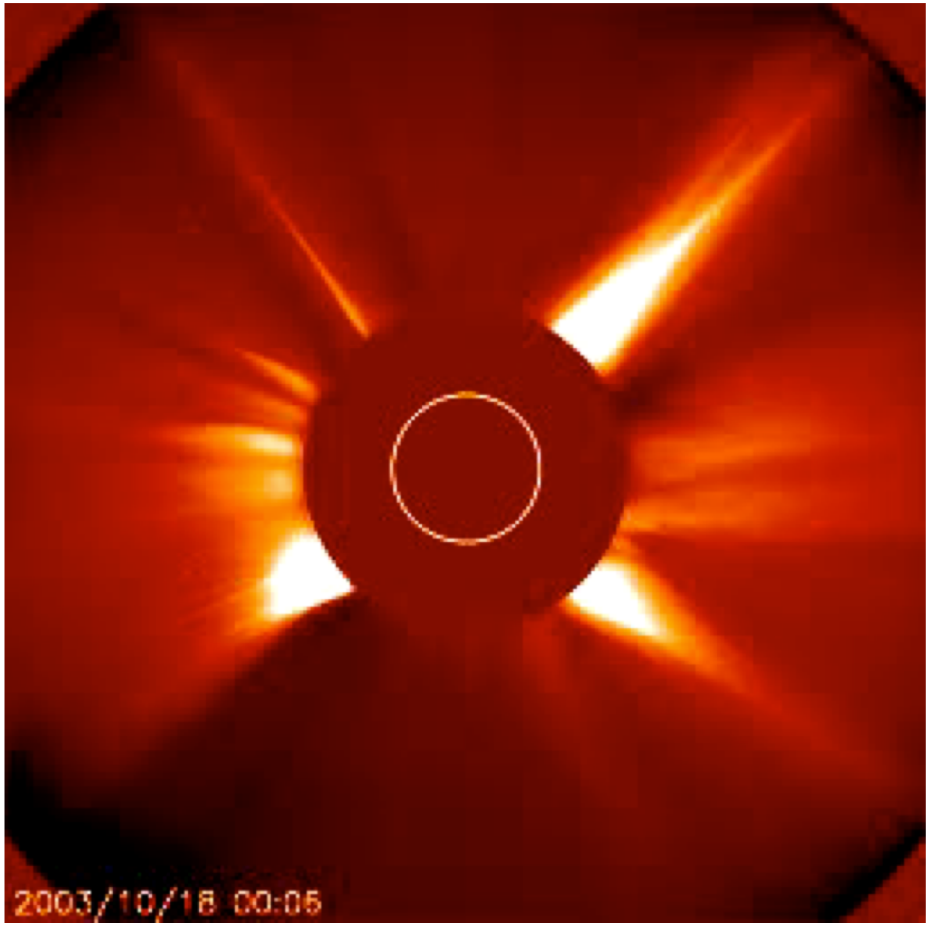

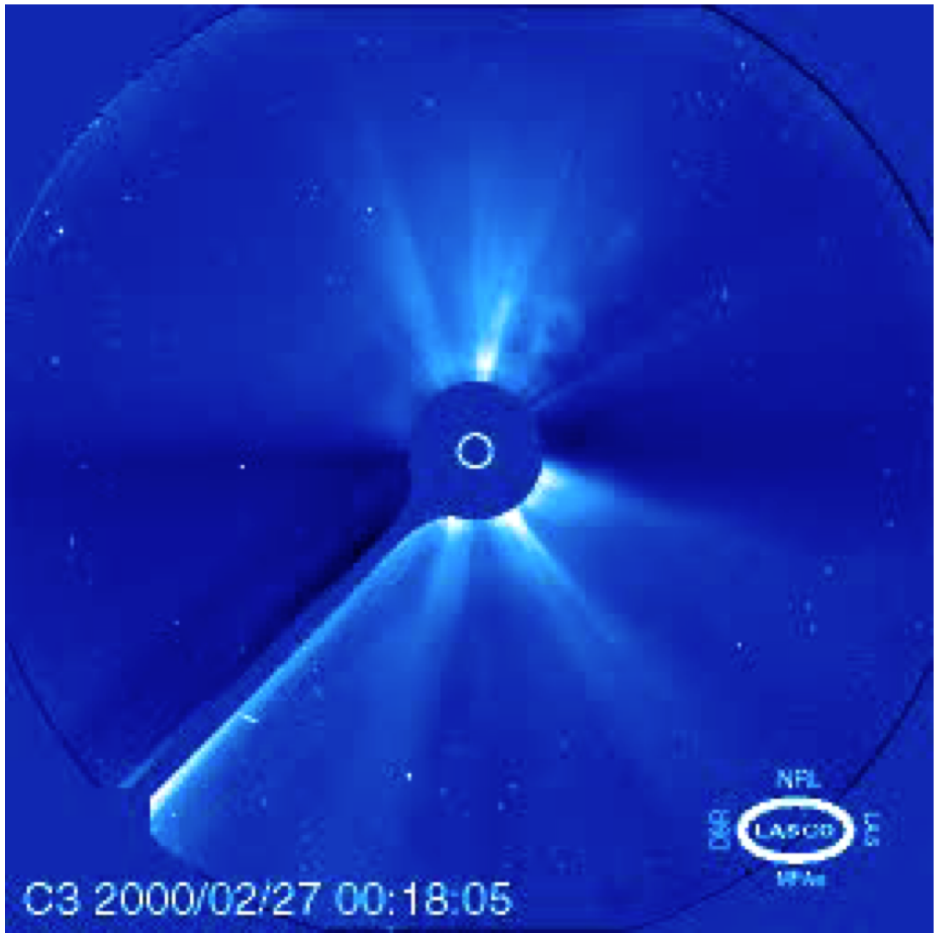

Large Angle and Spectrometric COronagraph (LASCO, 1995 -) observes CMEs from earth view, with the FOV in solar radii, C2: 1.5 - 6, C3: 3.5 - 30

CMEs best seen by coronagraphs

WISPR/PSP
the distance

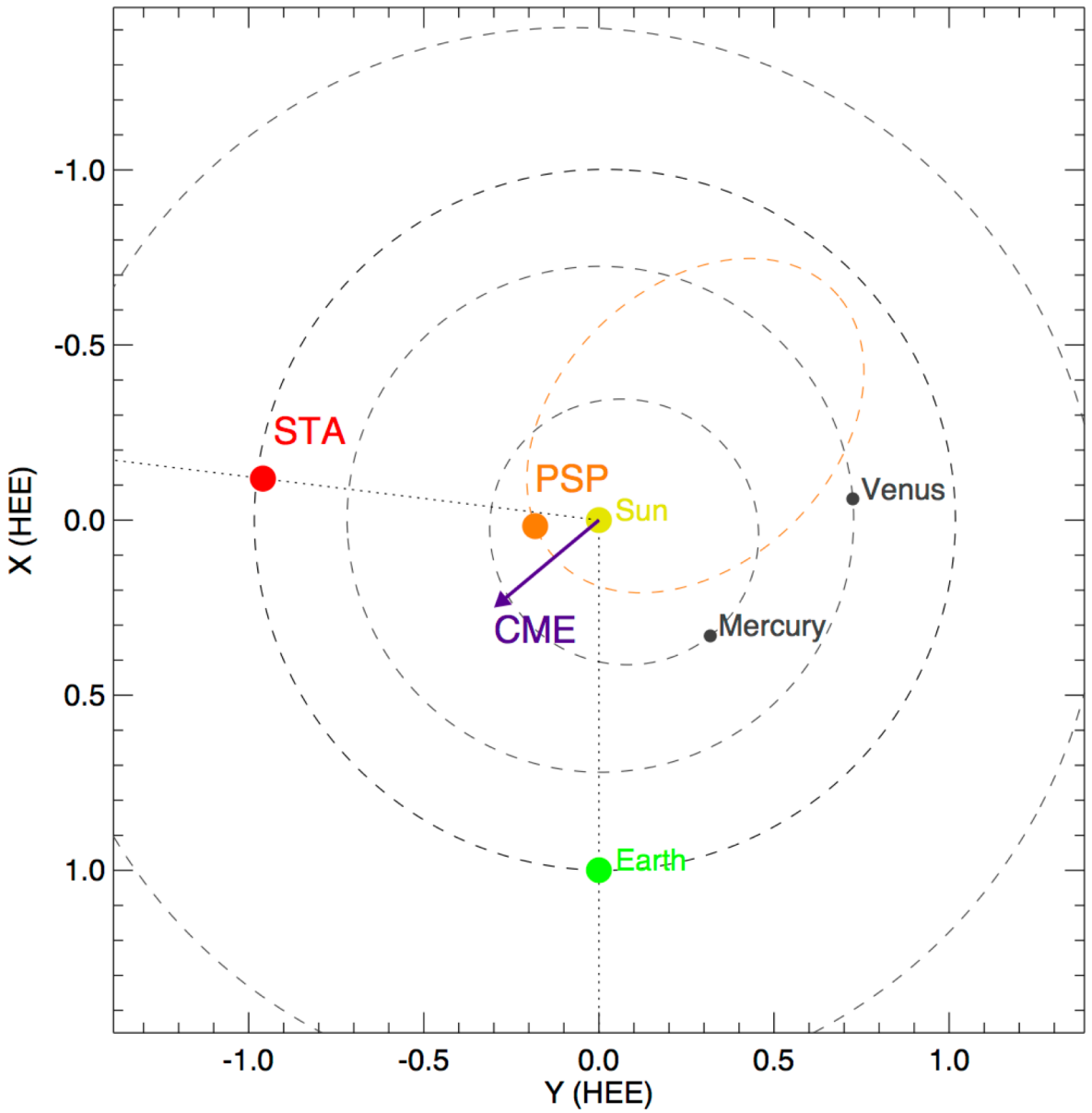

UVI (0 – 1.7),
, HI (– 1AU)
craft A & B.

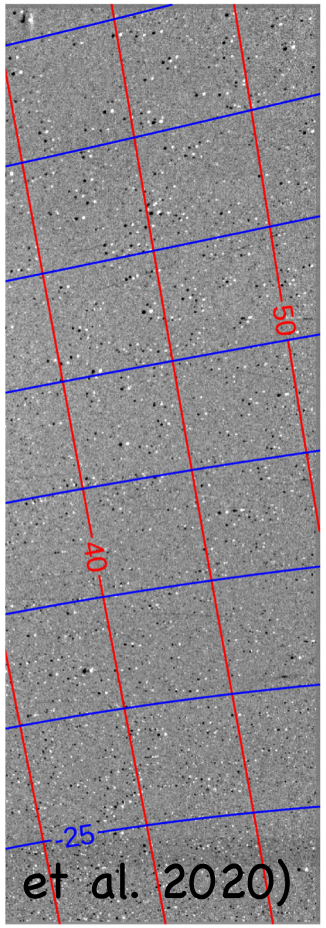

et al. 2020)

Early observations and models of CMEs

CMEs observed during solar eclipses showing their three-part structure. (Hundhausen et al, 80-90s, Low, Gibson et al., Low 1996).

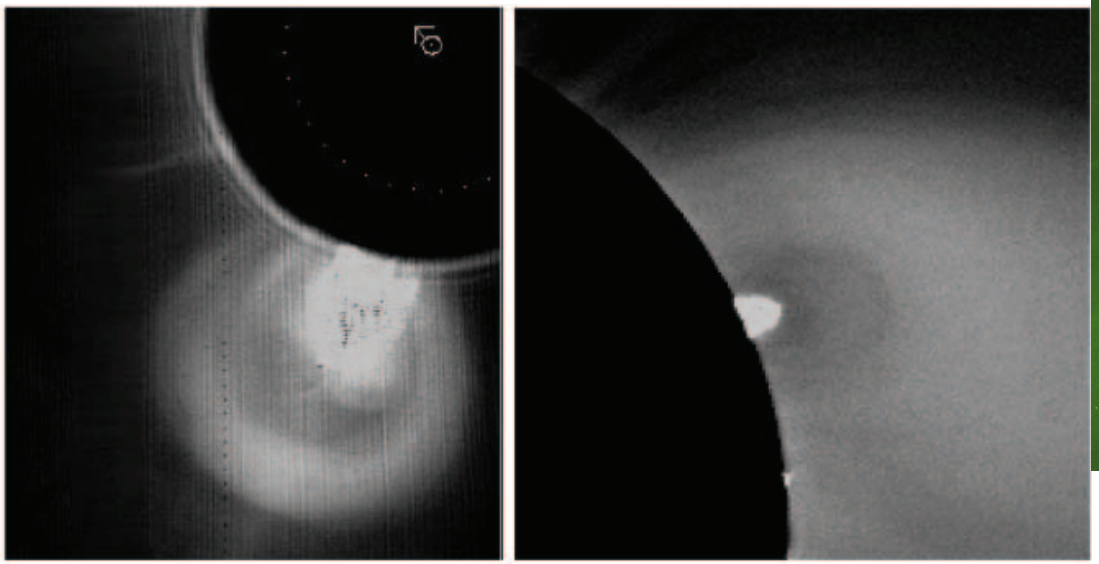

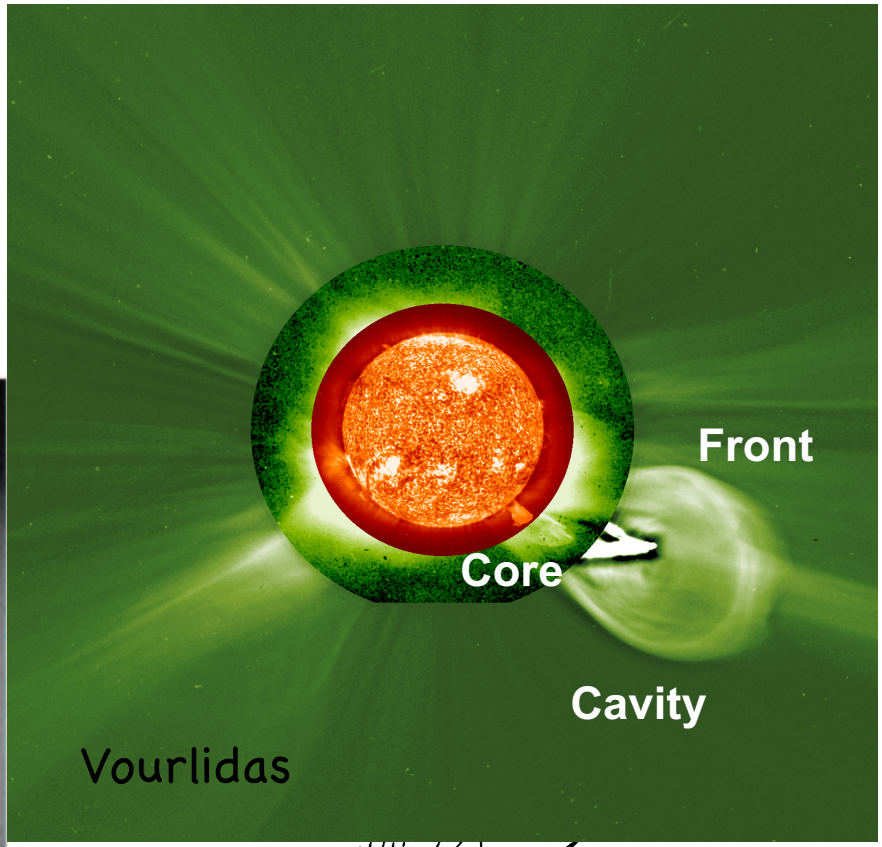

FIG. 1.—Three-part structures in white-light-containing cavities. Three-part CME in eruption (*left*) on 1980 August 18 (High Altitude Observatory/*Solar Maximum Mission* coronagraph). Quiescent prominence plus cavity (*right*) is seen in the 1988 March 18 Philippines eclipse image (National Center for Atmospheric Research/High Altitude Observatory Newkirk White-Light Coronal Camera [WLCC] telescope).

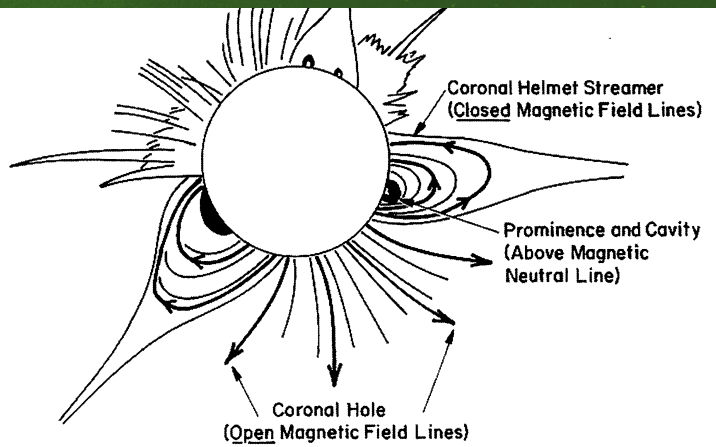

CME as a magnetic flux rope

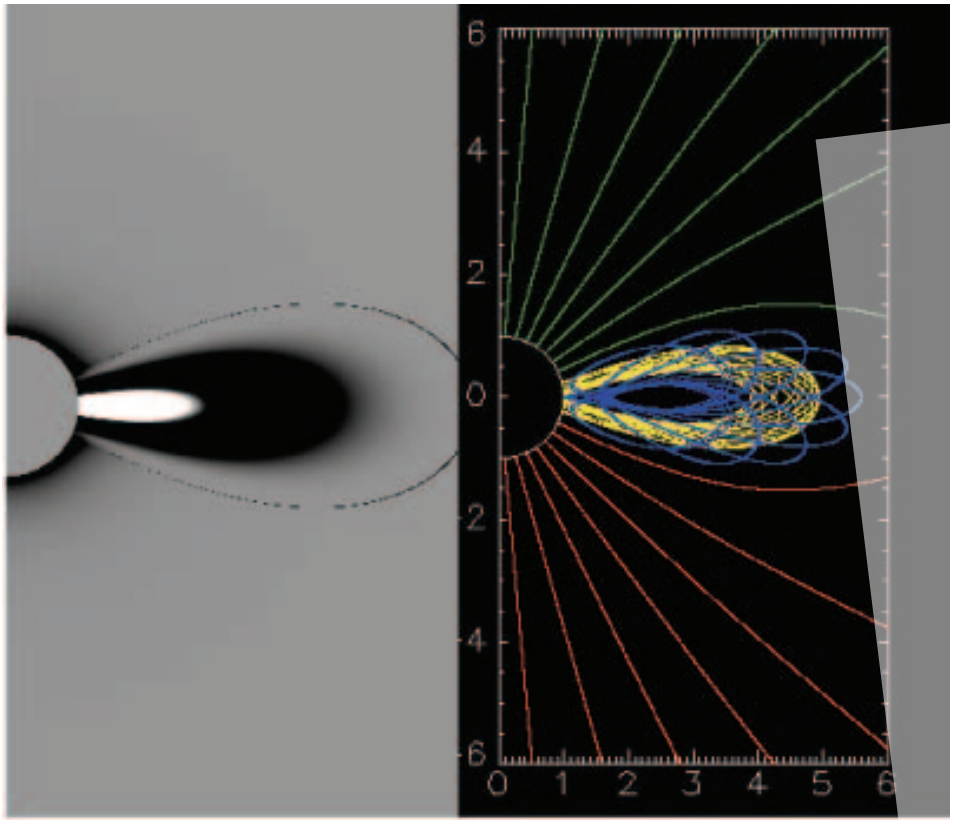

Gibson-Low model

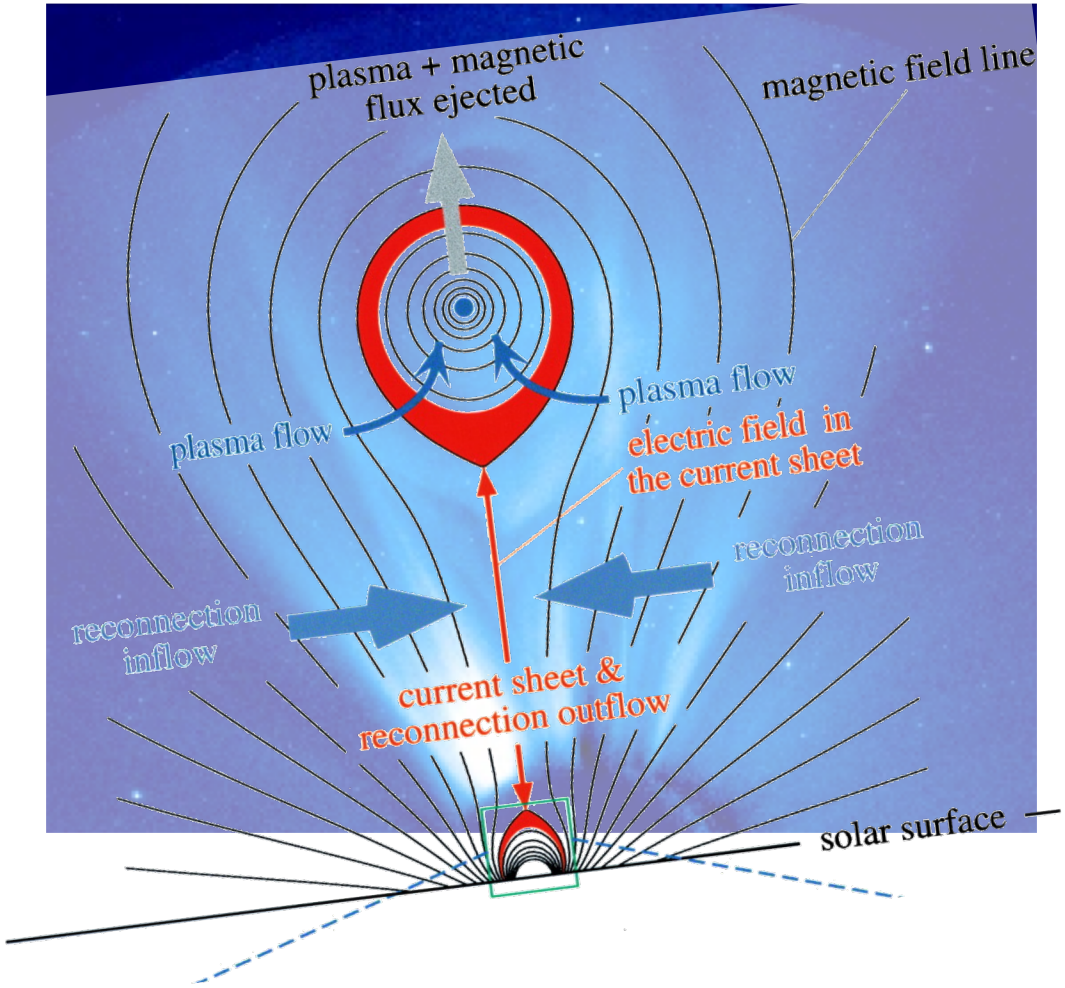

Forbes-Lin model

Magnetic Cloud, an Interplanetary CME

- 1954 Morrison: unusual magnetized clouds of plasma emitted by the active sun.
- 1958 Cocconi et al.: magnetic loop or bottle anchored in the sun.
- 1958 Piddington: magnetic bubble detached from the sun by reconnection.
- 1959 Gold: shocks preceding these magnetic loops
- 1980-81 Burlaga: first coined "magnetic cloud"
- 1990, 1997, Lepping: magnetic cloud properties

(Burlaga et al, 1981, JGR, 86, 6673-6684)

In-situ measurements of Magnetic Cloud

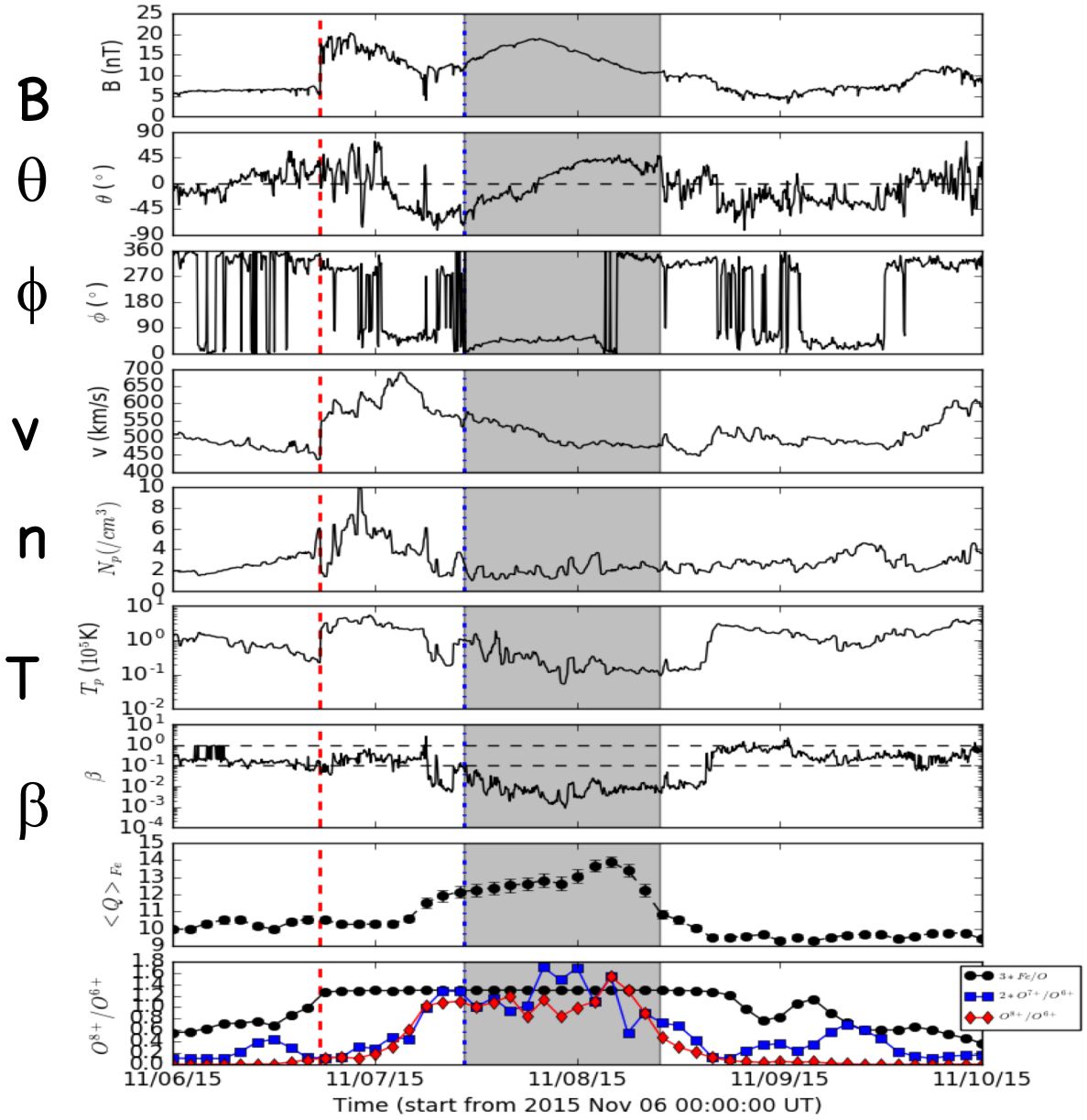

Liu R. et al. 2017

Tightly wound helix
B: 10 - 100 nT

Low temperature
T : 10^5 K, n: 10 – 100 cm^{-3}, β: 0.01 – 0.1

Higher speed than ambient solar wind
v: 300 - 800 km s^{-1}

Preceded by shocks and sheaths

(Burlaga et al 1981; Lepping et al. 1990)

In-situ measurements of Magnetic Cloud

B, B_x
B_y, B_z

v

n, T

β

P

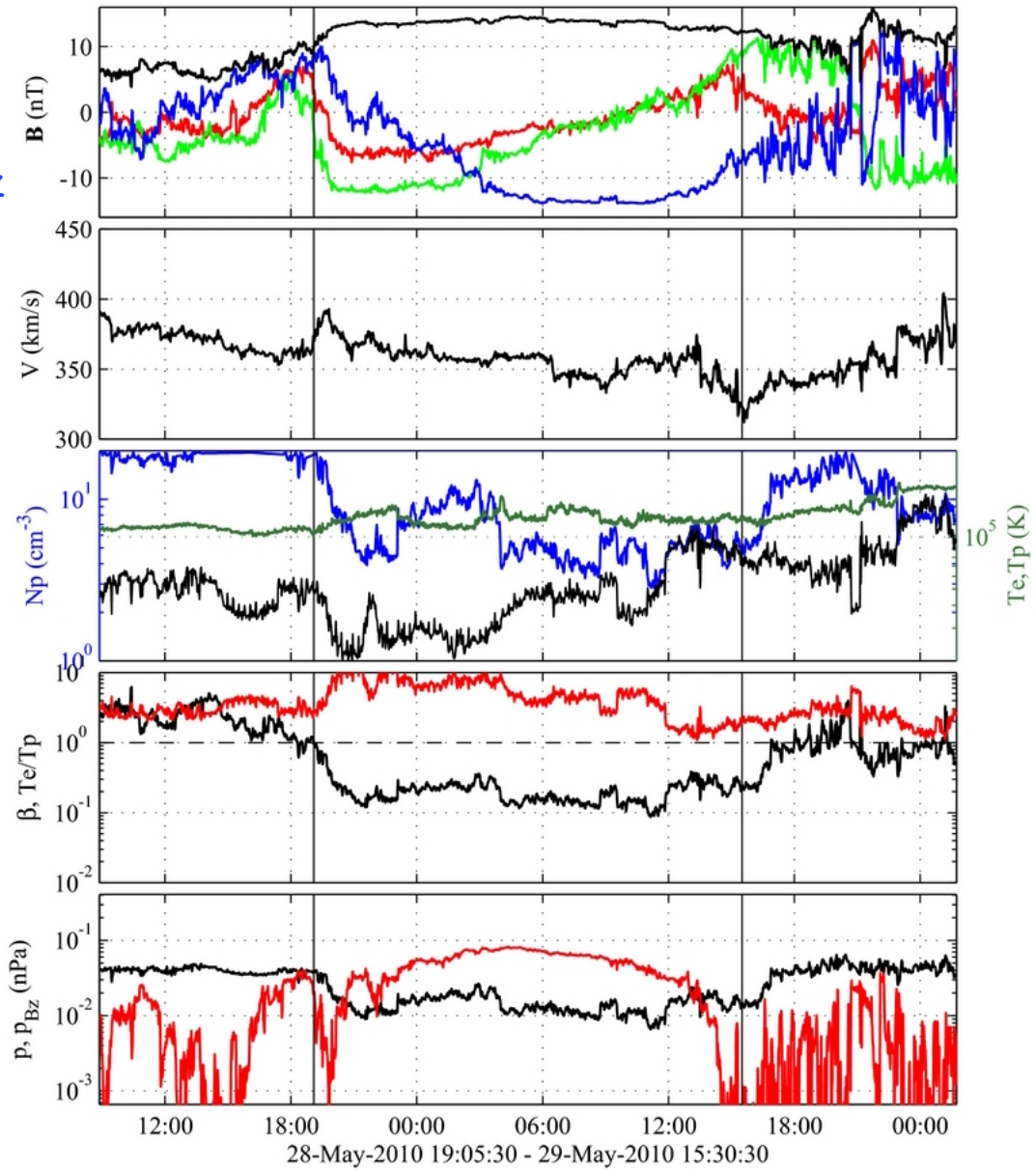

Hu et al. 2014

Tightly wound helix
B: 10 - 100 nT

Low temperature
T : 10^5 K, n: 10 – 100 cm^{-3}, β: 0.01 – 0.1

Higher speed than ambient solar wind
v: 300 - 800 km s^{-1}

Preceded by shocks and sheaths

(Burlaga et al 1981; Lepping et al. 1990)

Magnetic Cloud: interplanetary flux rope

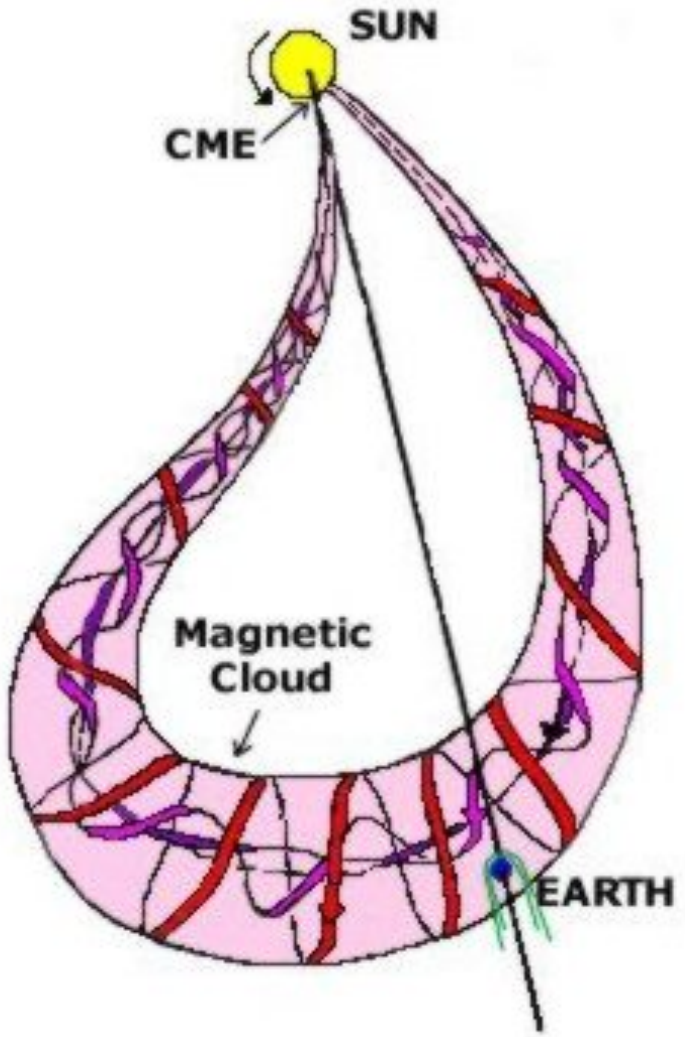

[After Marubashi]

Not to Scale

From in-situ observations, a flux rope may be reconstructed with various methods (Riley et al. 2004, Dasso et al. 2006 for a summary of these methods), assuming a 2d cylindrical structure of the CME flux rope, which is a force-free or magnetostatic solution.

MC flux rope: the Lundquist solution

$$\mathbf{B}_0(r) = B_0\left[J_0(\alpha r)\hat{\mathbf{z}} + J_1(\alpha r)\hat{\phi}\right]$$

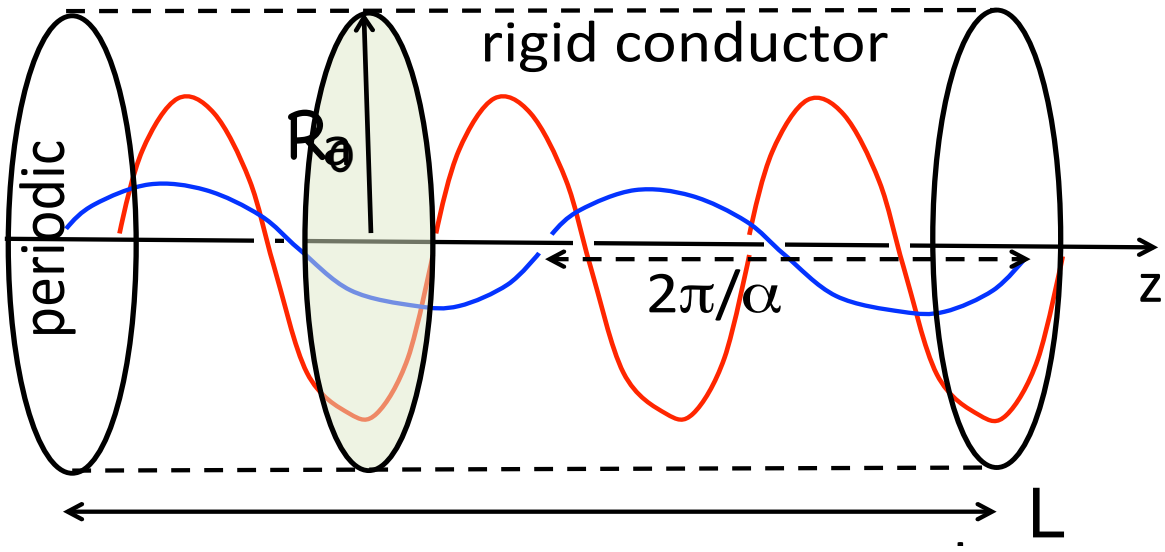

Least-squares fitting of the data points to determine parameters, including the rope axis orientation, radius, and axial field B_0.

(Lepping et al. 1990, Lynch et al. 2005)

toroidal flux:

$$\Phi_t = \iint B_z r dr d\phi$$

poloidal flux:

$$\Phi_p = \iint B_\phi \, dr dl$$

magnetic helicity:

$$H_m = \int \vec{A} \cdot \vec{B} \, d^3x$$

$$= \frac{1}{\alpha}\int B^2 d^3x$$

magnetic twist:

$$T = \frac{lB_\phi}{rB_z}, \; \tau = \frac{T}{2\pi}$$

MC flux rope: the Lundquist solution

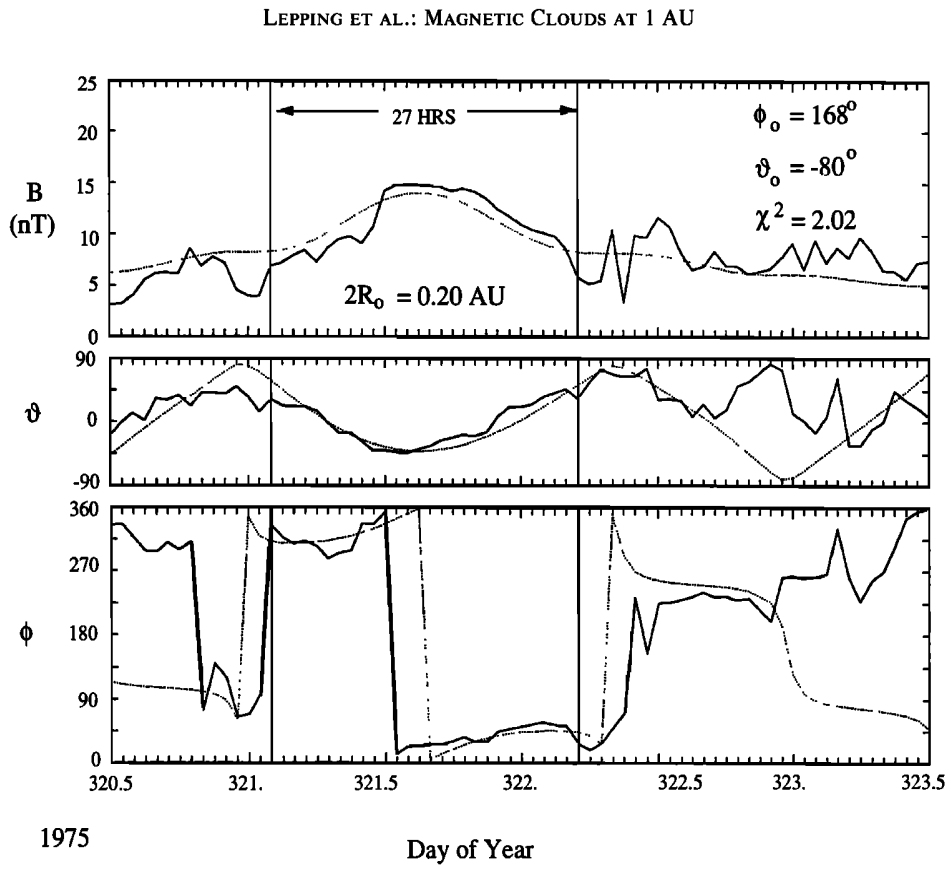

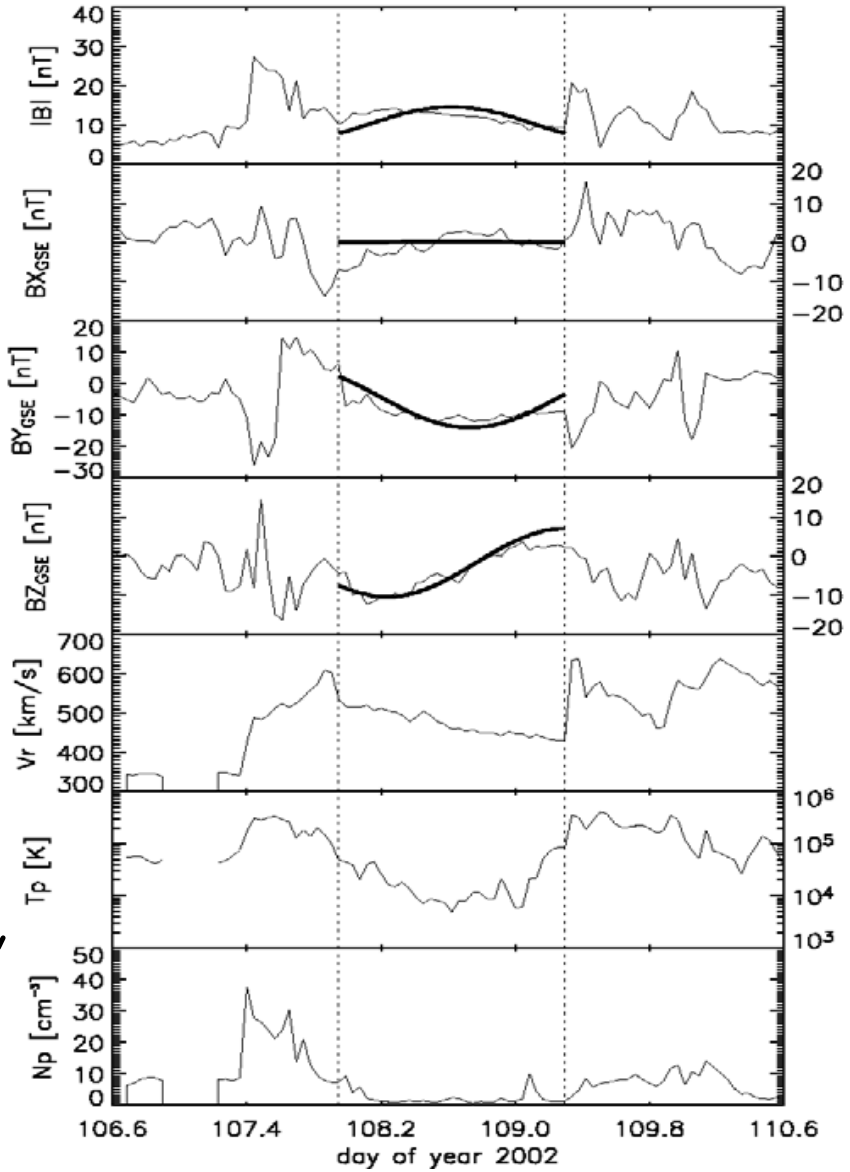

18 MC flux ropes by Lepping et al. 1990, and 132 MC ropes by Lynch et al. 2005)

MC flux rope: the GS solution

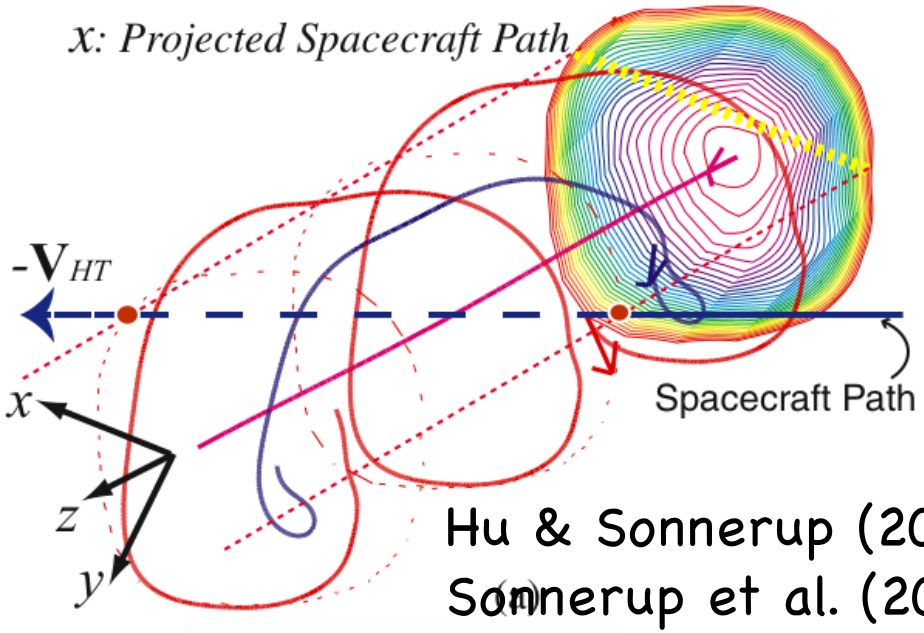

Hu & Sonnerup (2002)
Sonnerup et al. (2006)

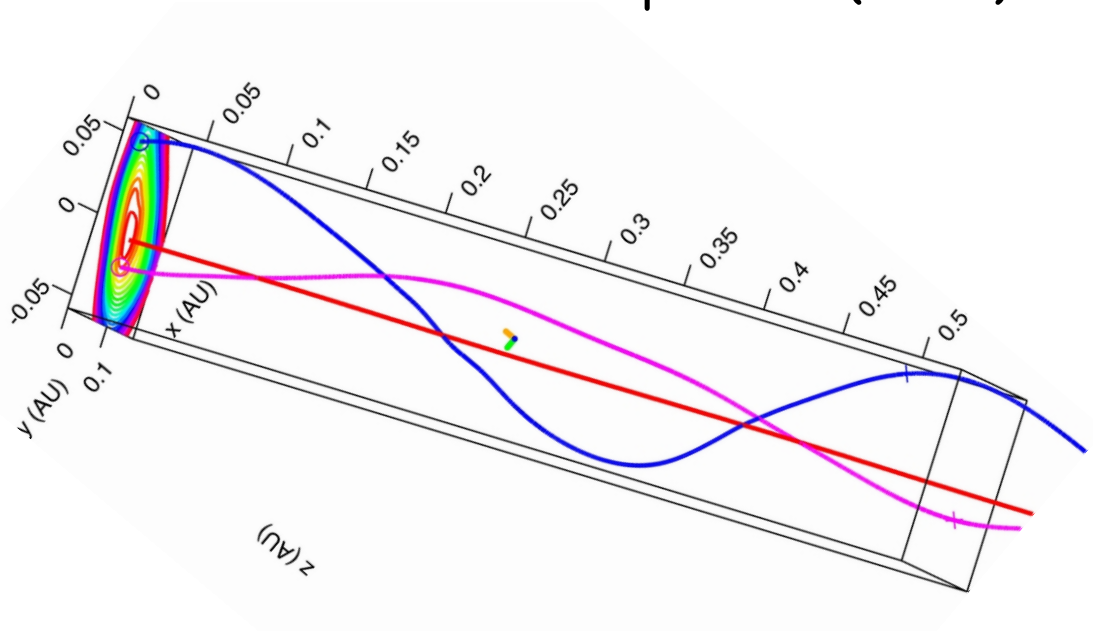

2d magnetostatic non-force-free Grad-Shafranov equation

$$\vec{\nabla} p = \vec{j} \times \vec{B}$$

$$\vec{B} = \left(\frac{\partial A}{\partial y}, -\frac{\partial A}{\partial x}, B_z(A) \right)$$

$$P_t(A) = p(A) + B_z^2 / 2\mu_0$$

$$\frac{\partial^2 A}{\partial x^2} + \frac{\partial^2 A}{\partial y^2} = -\mu_0 \frac{dP_t}{dA}$$

$$\Phi_t = \iint B_z dx dy$$

$$\Phi_p = |A_m - A_b| L$$

$$\tau = 1AU / Lz$$

MC flux rope: the GS solution

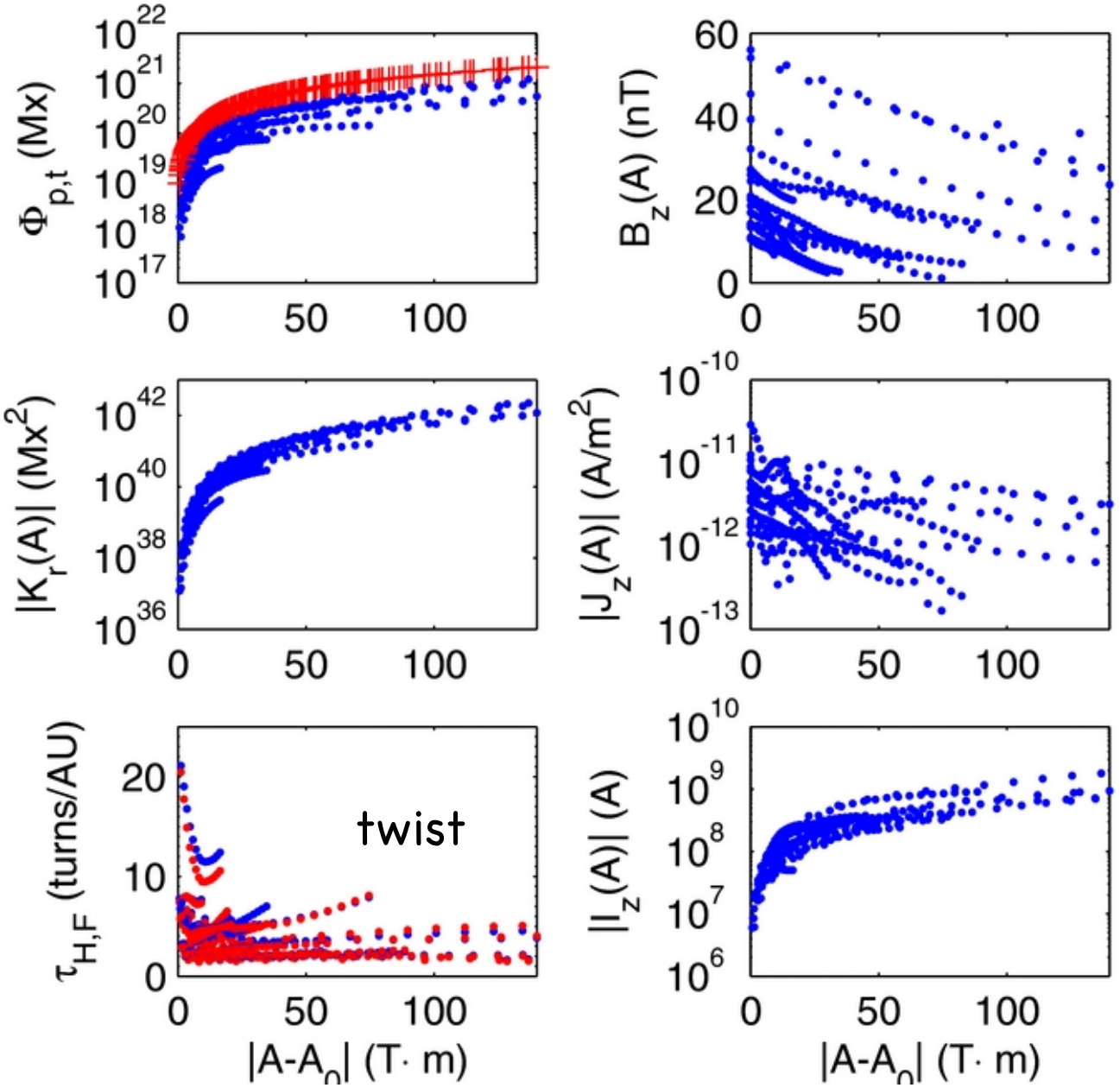

MC flux ropes carry an average twist of $\tau > 3$ per AU. (Hu et al. 2014, 2015; Kahler et al. 2011).

Hu et al. (2014)

Field line length of MC flux rope

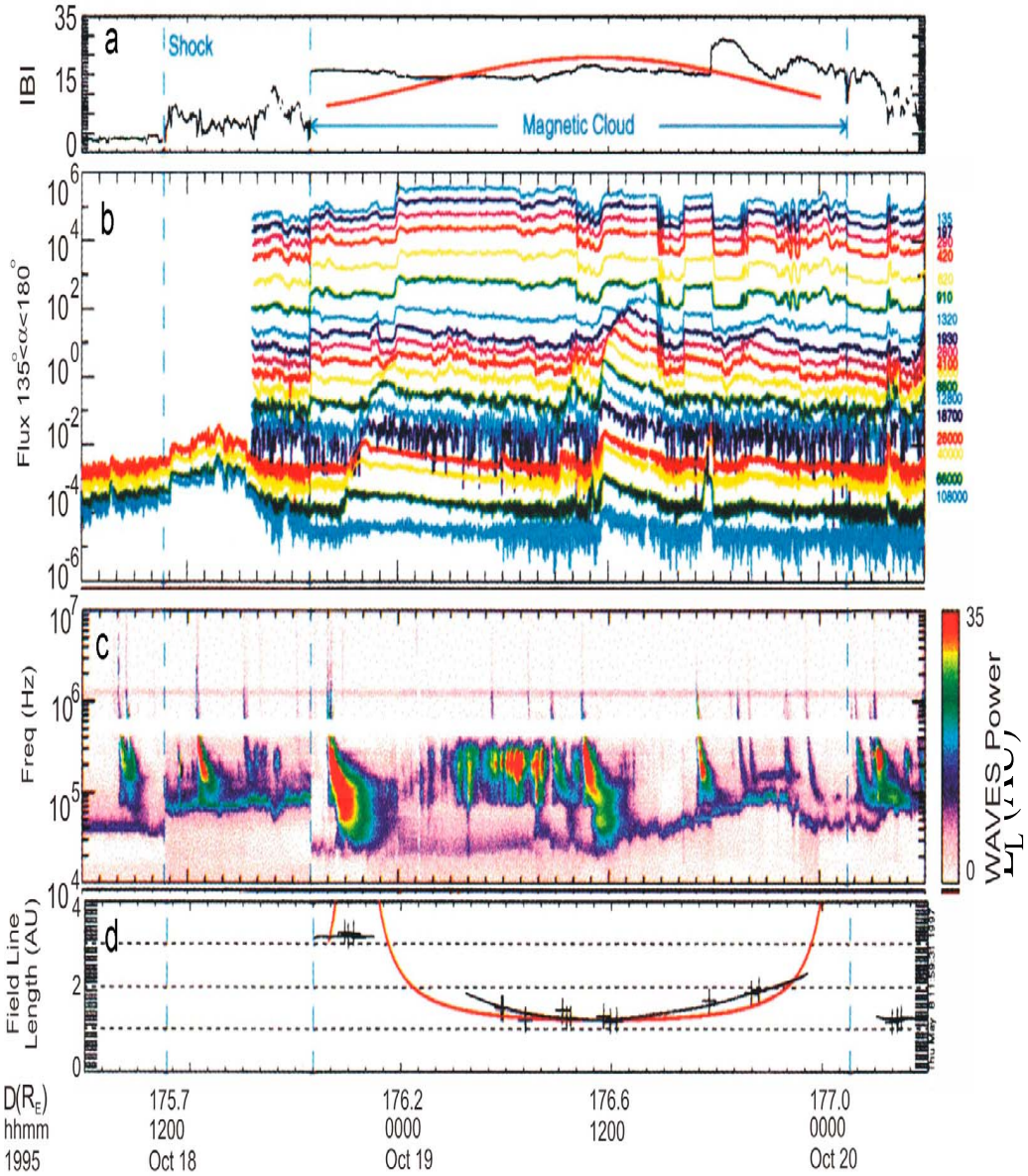

Lengths of MC field lines are also measured from electron travel times, $L_e = v_e \Delta t$, to compare with models (Larson et al 1997, Kahler et al 2011, Hu et al. 2015)

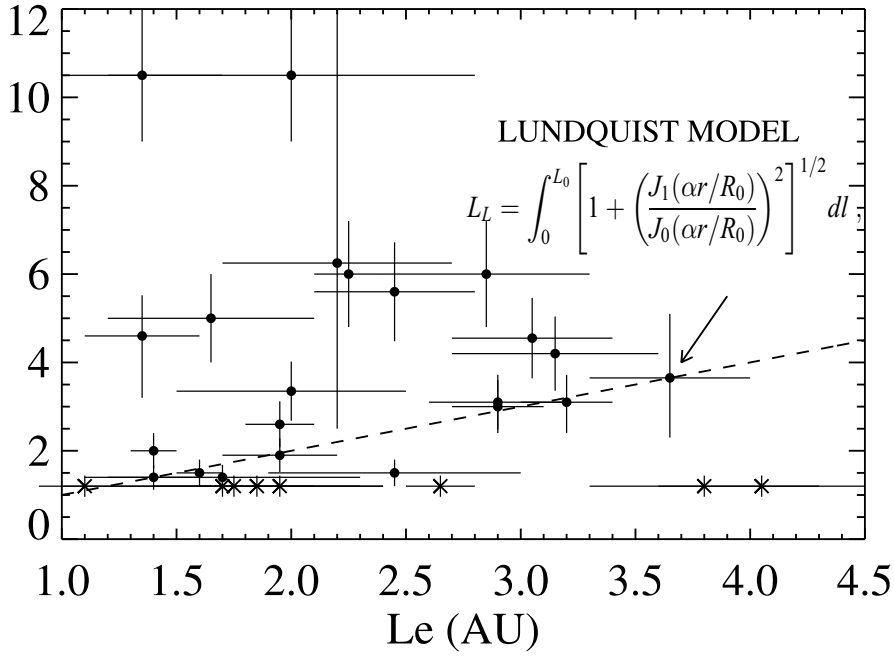

Figure 1. Composite panel of particles and fields measurements on the Wind spacecraft in the 19–20 October

properties of MC flux ropes

property	typical values at 1 AU
cross-sectional radius (a)	0.1 – 0.5 AU
axial (toroidal) flux	$10^{19\text{-}21}$ Mx
azimuthal (poloidal) flux per AU	$10^{20\text{-}22}$ Mx
magnetic helicity per AU	$10^{40\text{-}44}$ Mx^2
magnetic twist per AU	3 – 5 turns, or more

(Lepping et al. 2000, Lynch et al. 2005, Kahler et al. 2011, Hu et al. 2014)

What drives a CME flux rope?
How is the CME flux rope formed?
How much energy is carried away by a CME?

association with solar source regions

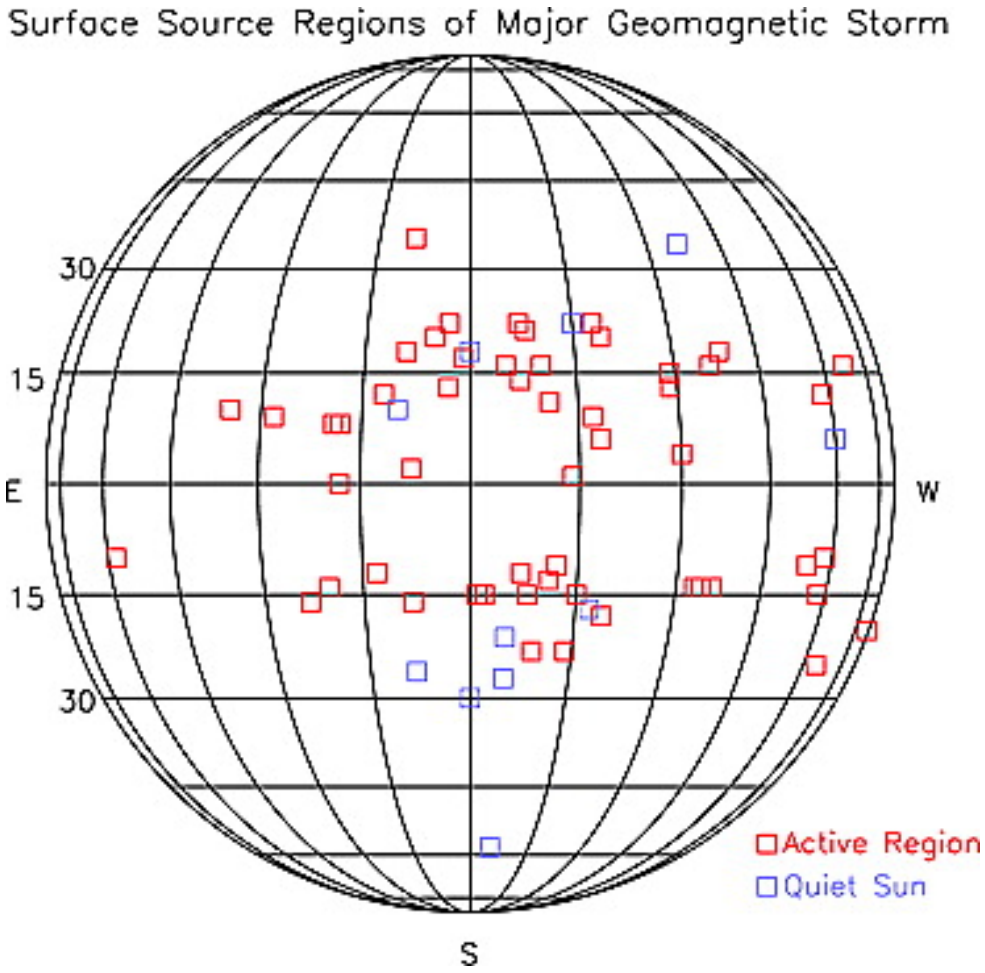

Zhang et al. (2007)

CDAW (1996-2005) identified solar source for 88 geomagnetic storms (Dst < -100 nT), 46 being MCs.

# of MCs (46)	Solar Source
28 (61%)	Active Regions
8 (17%)	Quiet Sun
10 (22%)	unknown

eruption by current driven instabilities

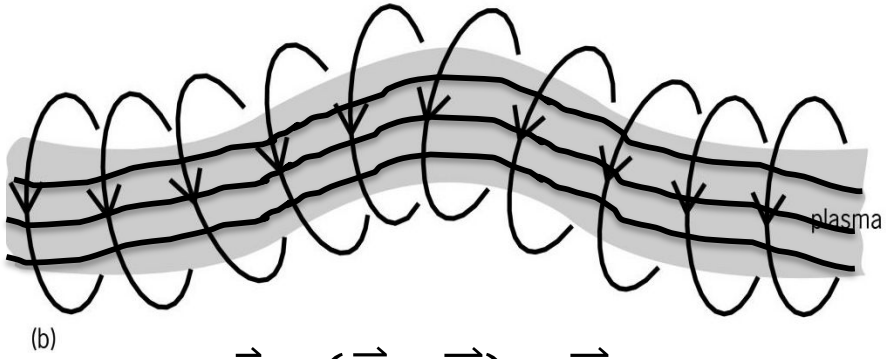

$$\vec{F} \sim (\vec{\nabla} \times \vec{B}) \times \vec{B}$$

Kink instability: competition of magnetic pressure gradient and tension force, defined by the twist $T = lB_\phi/(rB_z)$ (e.g. Hood & Priest 1981).

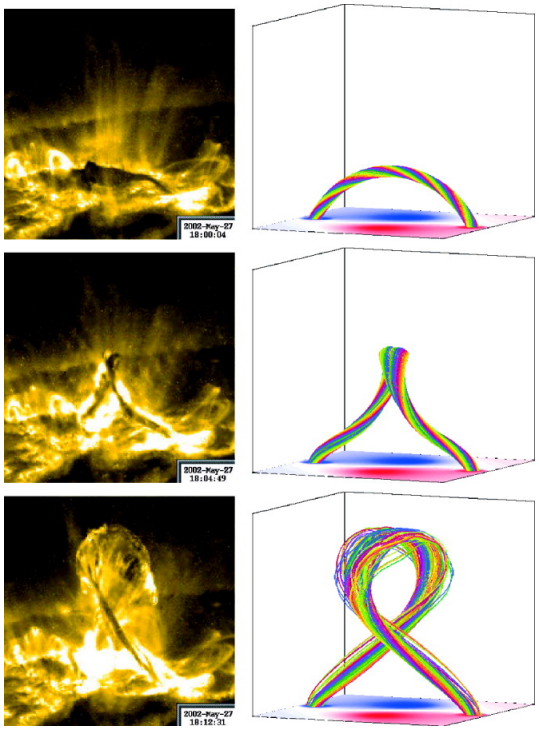

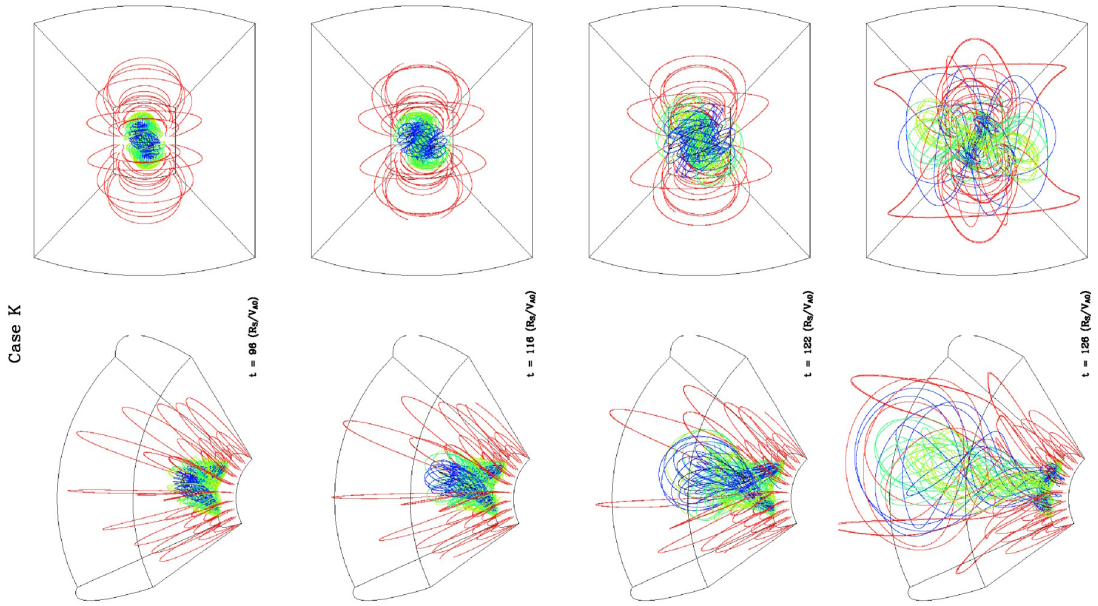

(Torok & Kliem 2005, Fan & Gibson 2007)

eruption by current driven instabilities

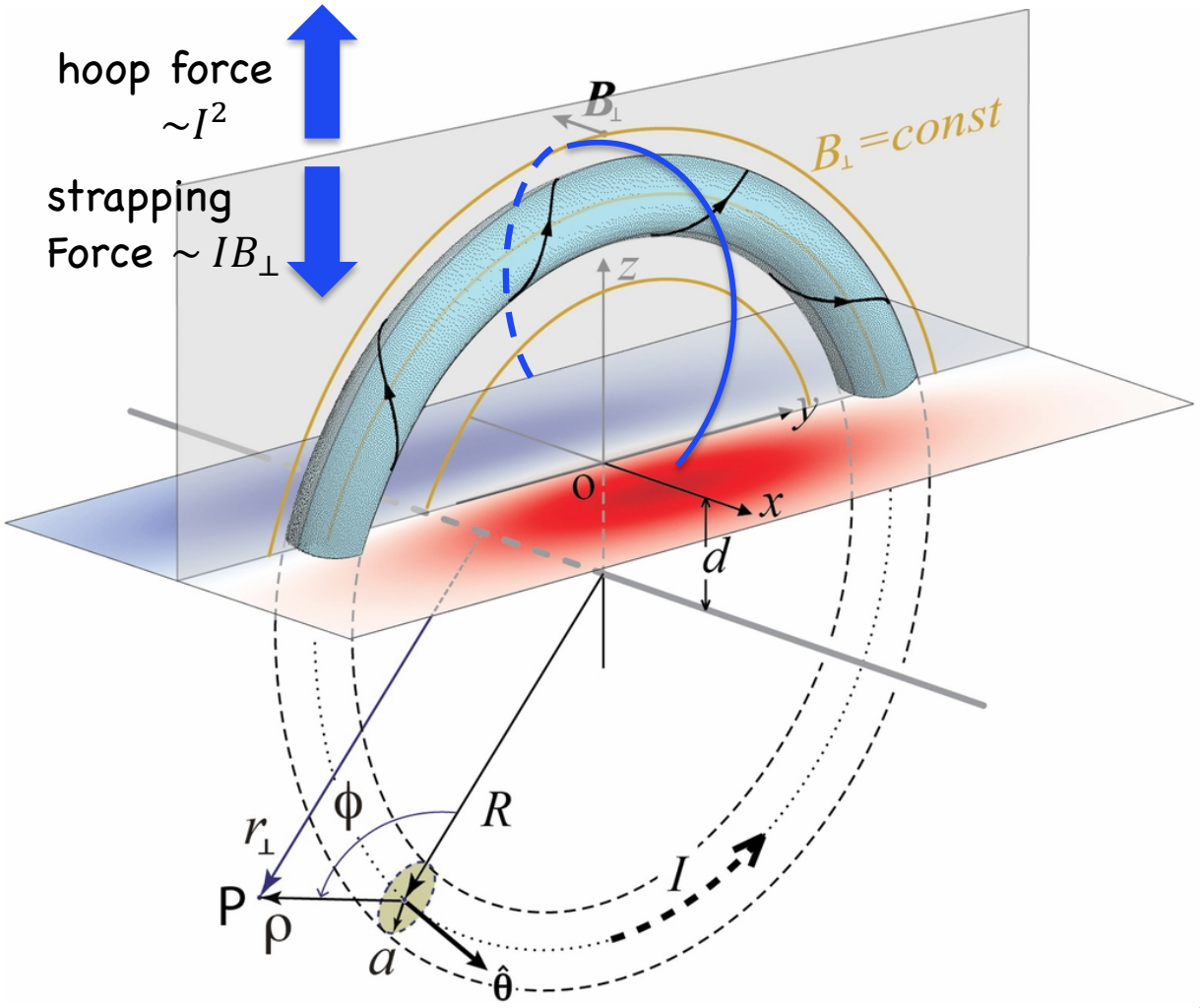

Titov et al. 2014

Torus instability: competition of current hoop force ($\sim I^2$) and Lorentz force by strapping field ($\sim IB_\perp$).

$$I \sim \frac{I_0 R_0}{R \ln\left[\frac{R}{a}\right]} \qquad \text{(Eq. 6.7)}$$

$$B_\perp \sim B_0 \left(\frac{R_0}{R}\right)^n$$

(e.g., Titov & Demoulin 1999; Kliem and Torok 2006; Isenberg & Forbes 2007; Fan & Gibson, 2007; Demoulin & Aulanier 2010)

reconnection may form flux ropes

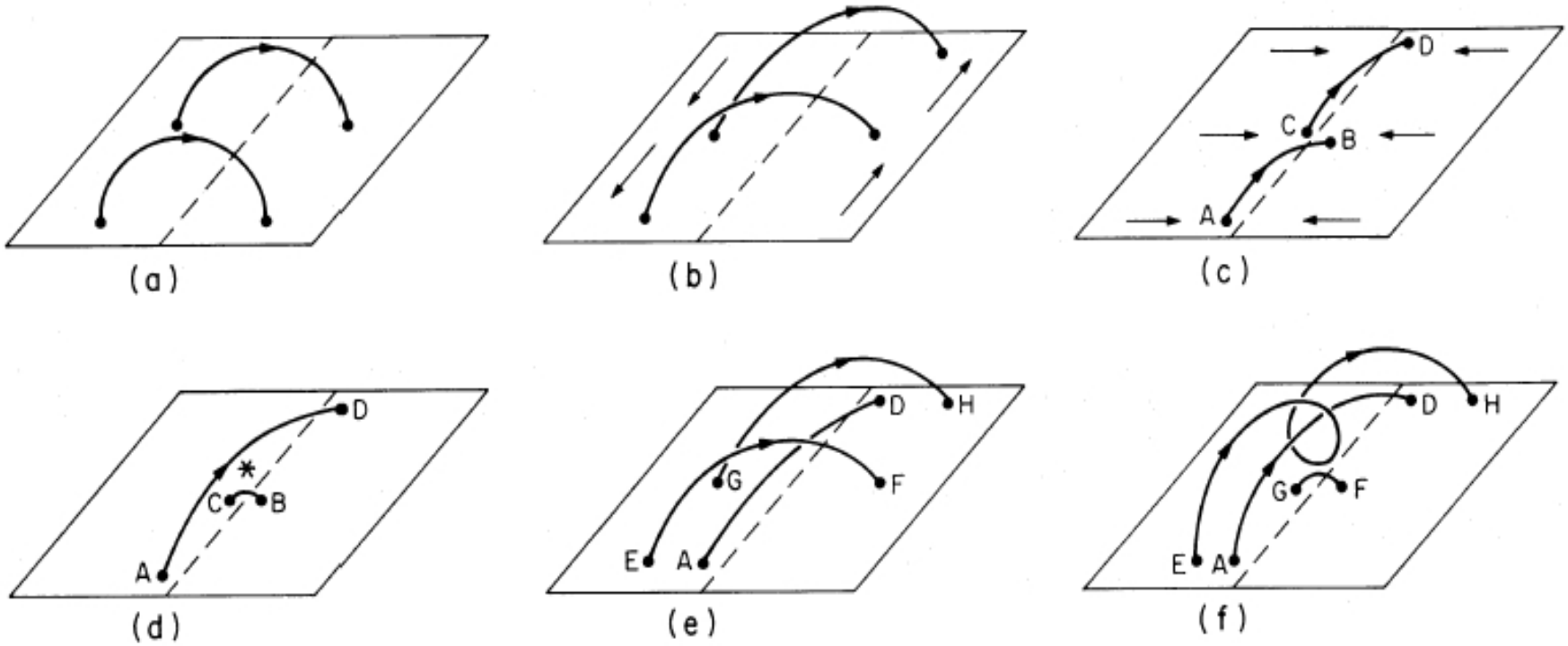

van Ballegooijen & Martens (1989)

Flux rope may emerge from below the photosphere, or may be formed by magnetic reconnection of a sheared arcade, transferring shear to twist.

reconnection may drive flux ropes

Resistive instability that cuts the tether, with the bonus to form the rope, as well as closed arcades.

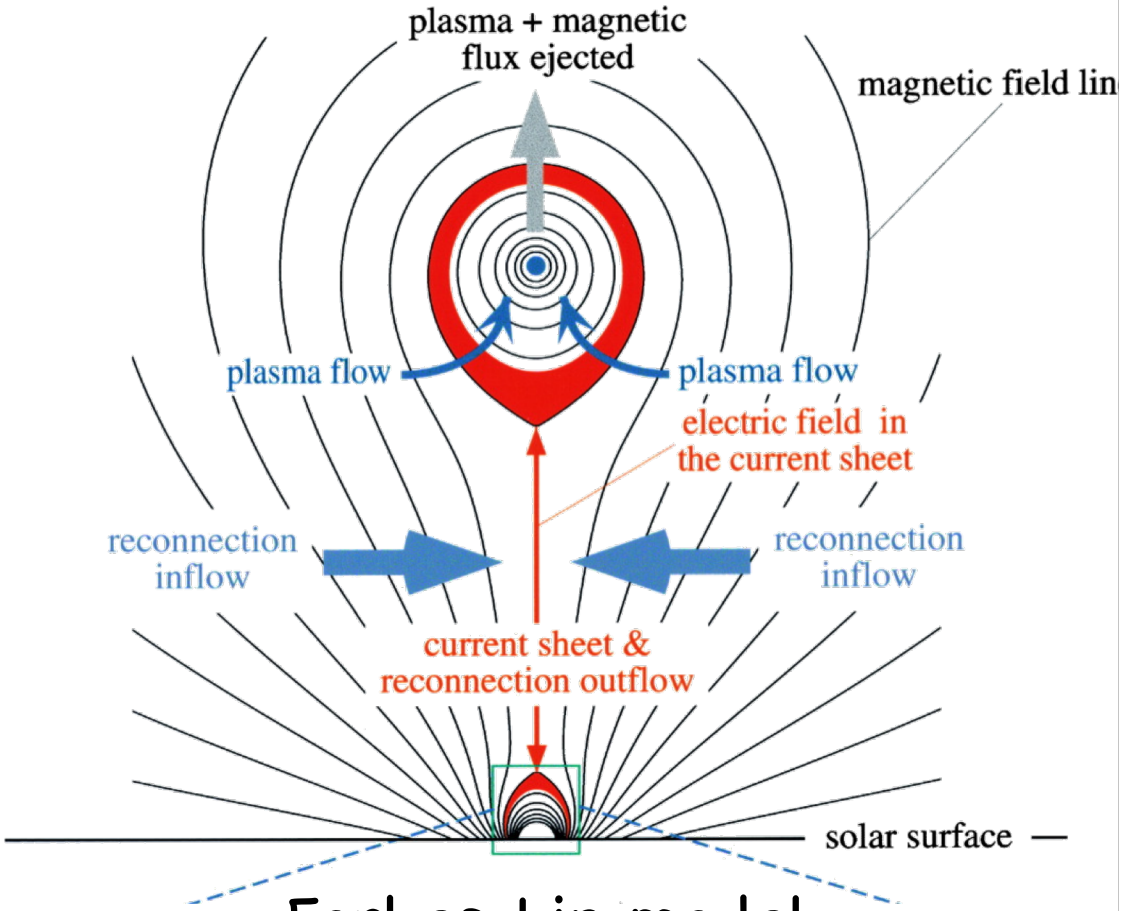

Forbes-Lin model

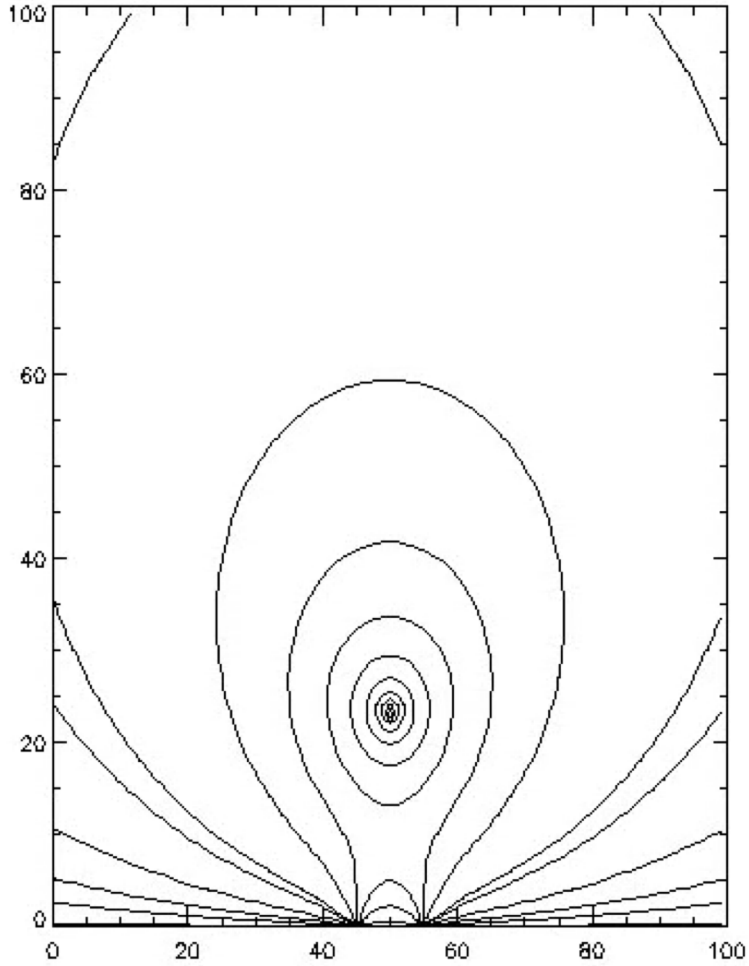

reconnection may be measured from flare ribbons

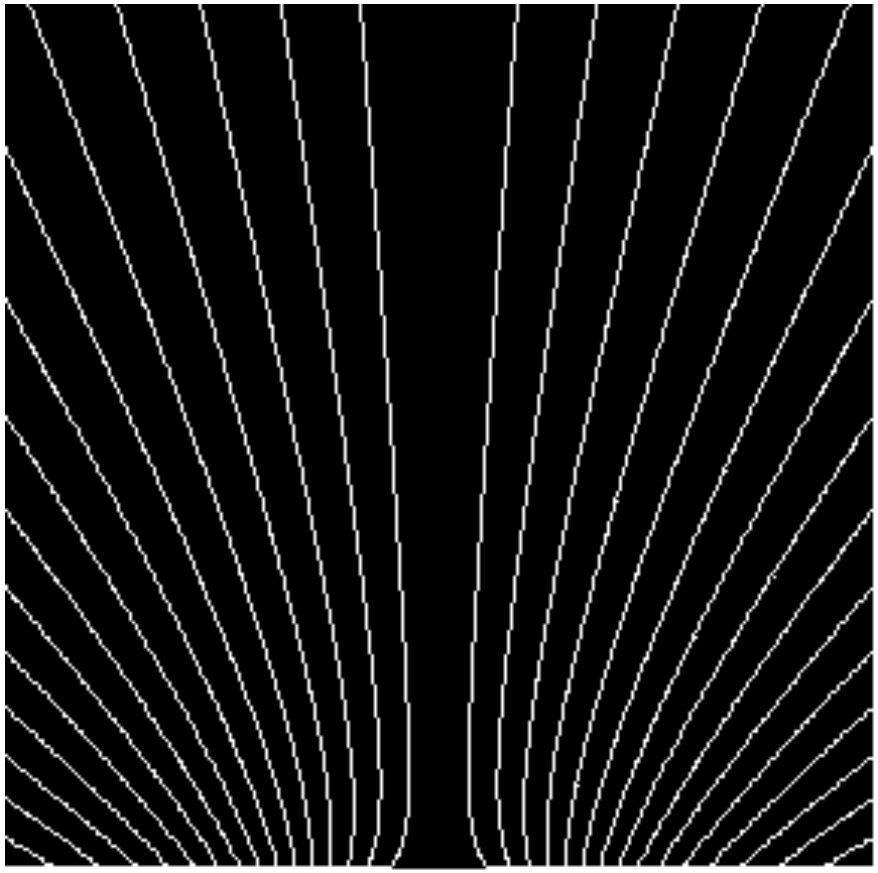

(Terry Forbes)

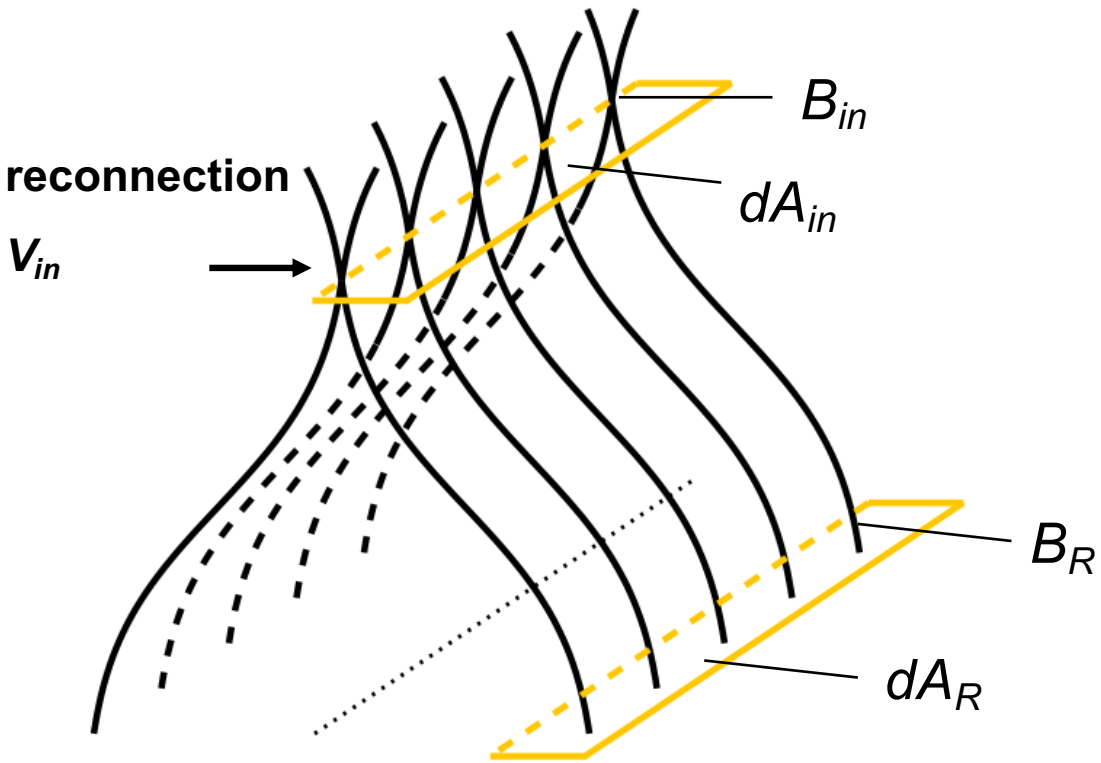

$$\frac{d\Phi_B}{dt} = -\oint \vec{E} \bullet d\vec{l} = \frac{d}{dt}\left(\int B_{in} dA_{in}\right) = \frac{d}{dt}\left(\int B_R dA_R\right)$$ (Forbes & Priest 1984)

multiple views of a flux rope eruption

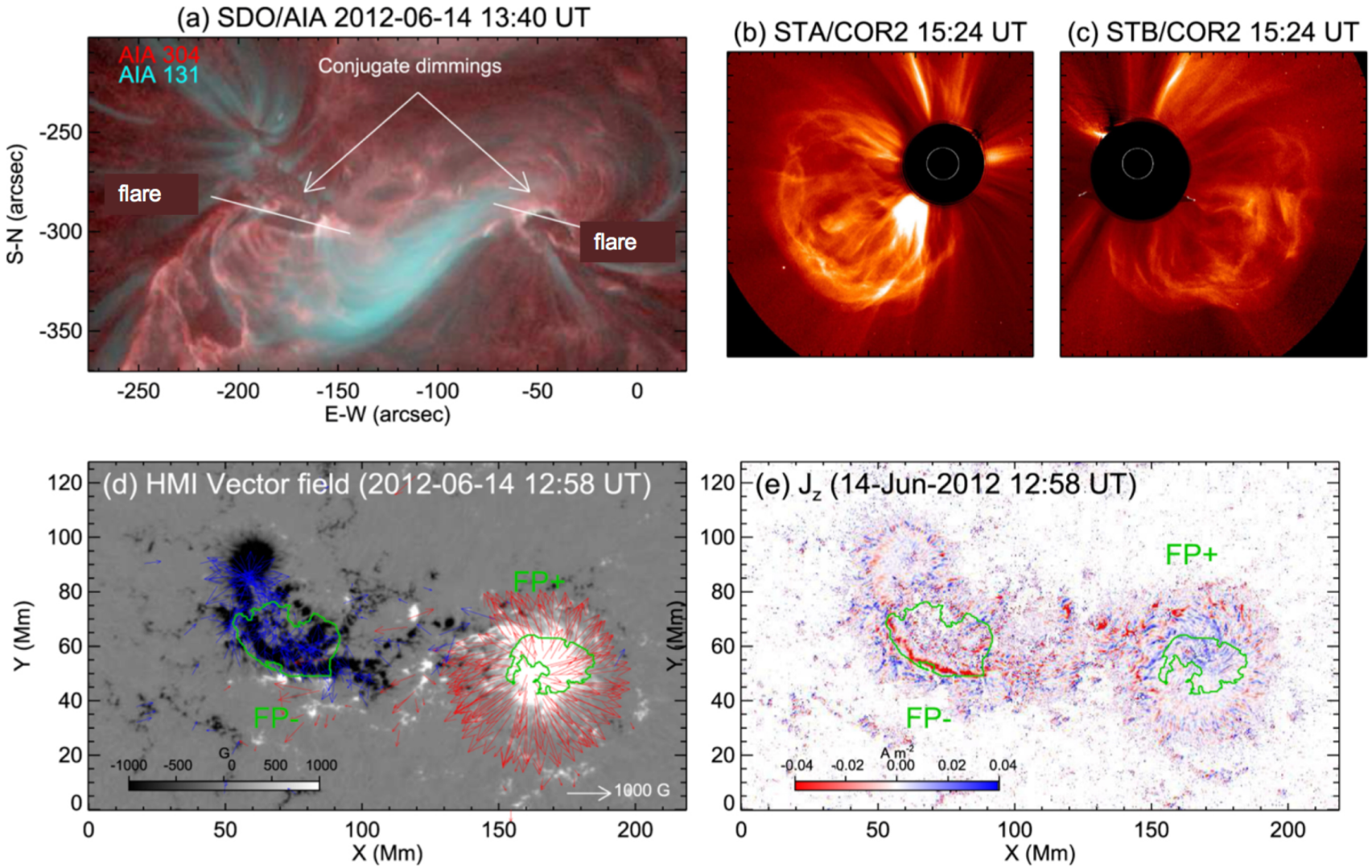

A CME flux rope on 2012-6-14, viewed from the limb by STEREO and on the disk by SDO (Wang et al. 2019).

evolution of host active region

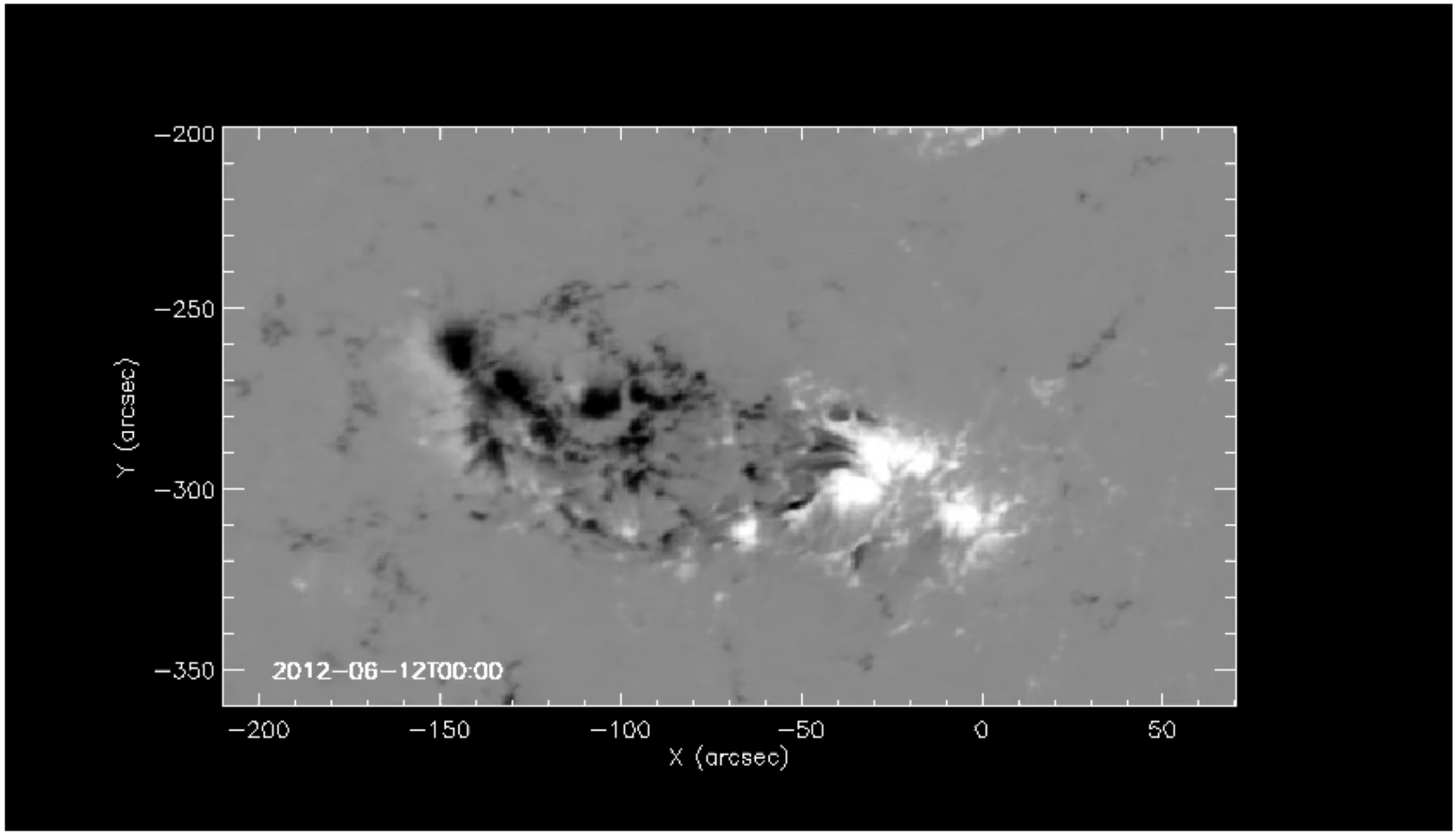

The host active region observed by HMI exhibits continuous sunspot rotation and shear motion.

magnetic properties of the flux rope

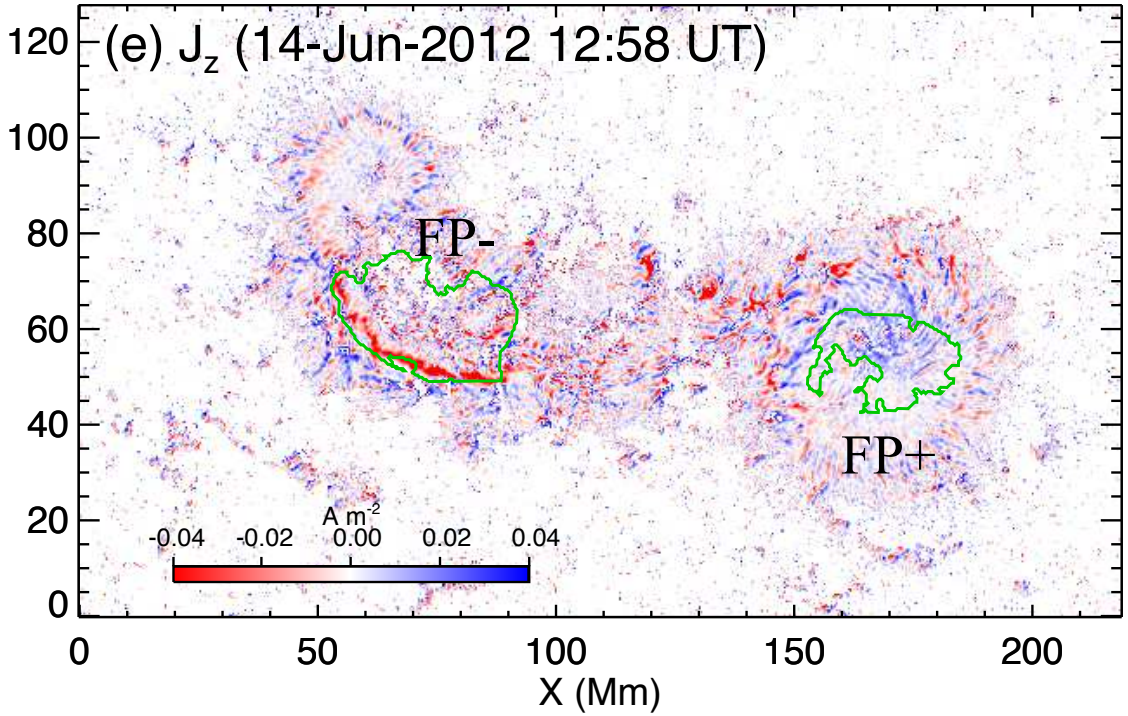

Conjugate dimmings map the feet of the flux rope at strong magnetic fields and vertical electric currents. At eruption, the estimated twist is close to 2 turns and helicity a few times 10^{42} Mx^2 (Wang et al. 2019).

	B_z	Φ_z	B_t	I_z
FP+	1500 G	4e21 Mx	1000 G	1.3/-0.5e12 A
FP-	-710 G	-3e21 Mx	500 G	-3.8/2.0e12 A

evolution of the flux rope toward eruption

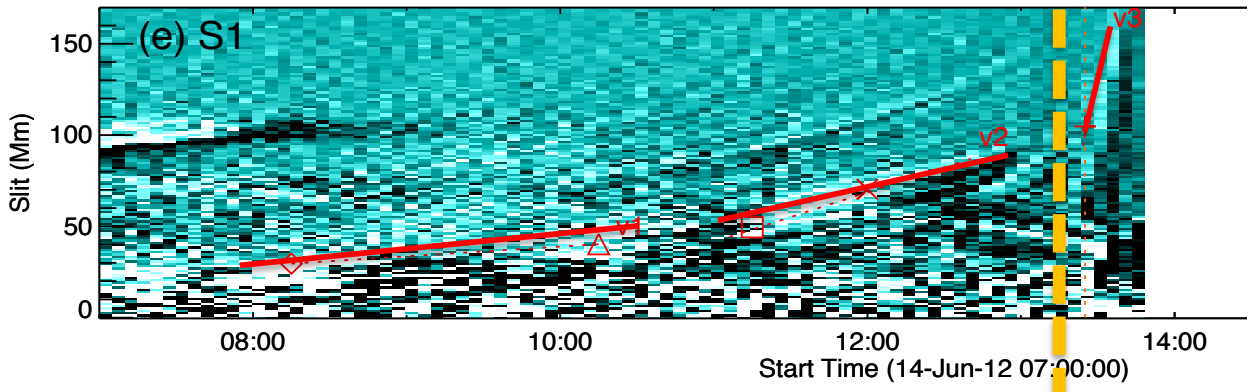

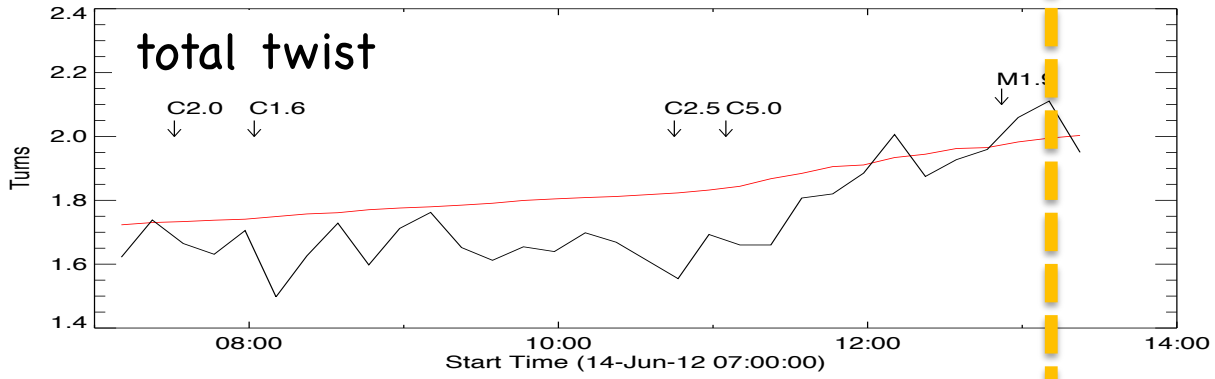

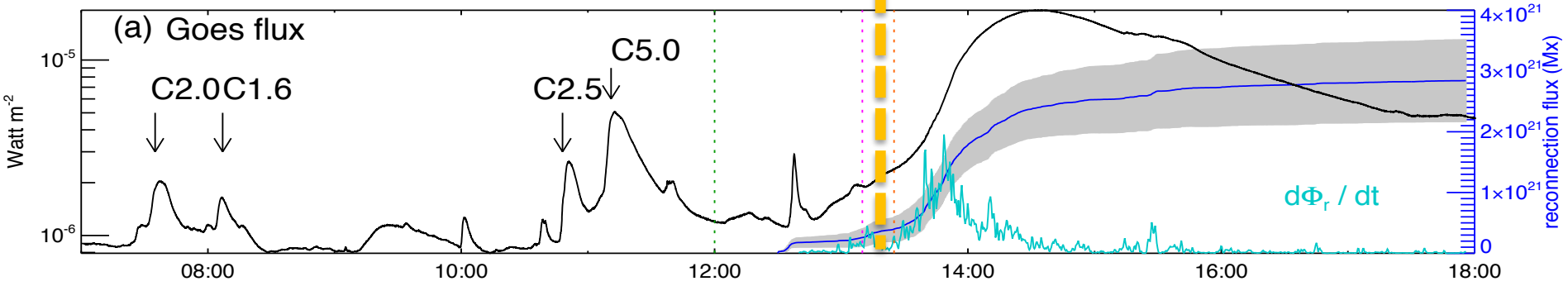

Flux rope rises in three stages, each preceded by flares (Wang et al. 2019).

modeling the magnetic flux rope

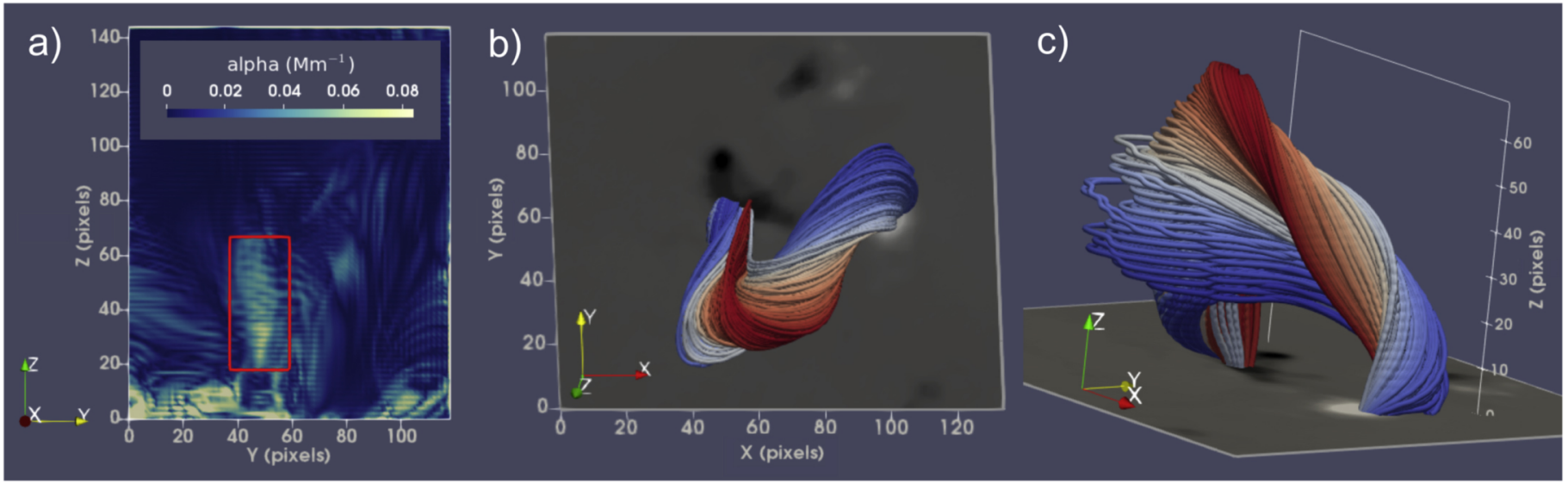

Numerical models are also employed to estimate properties of the flux rope and ambient field (James et al. 2018, Wang et al. 2019).

What forms flux rope? Shear motions? Reconnection?

What causes eruption? Kink instability? Torus instability? Reconnection?

Ideal and non-ideal mechanisms may interplay during the flux rope evolution, and convert free magnetic energy into mass motion.

height, velocity, and acceleration of CMEs

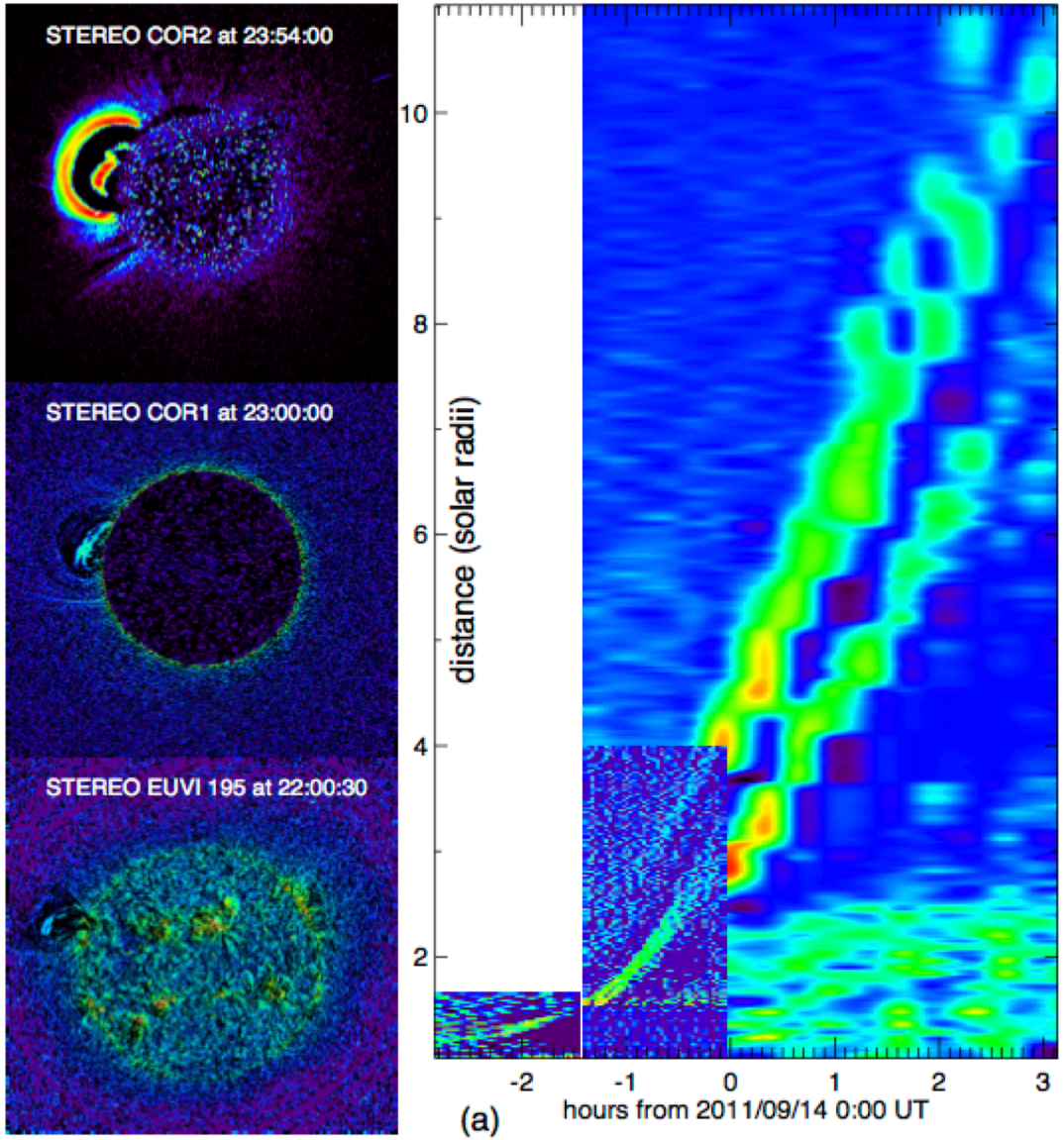

tracking different parts of the CME in a time-height plot, or J-map (Sheeley et al. 1999).

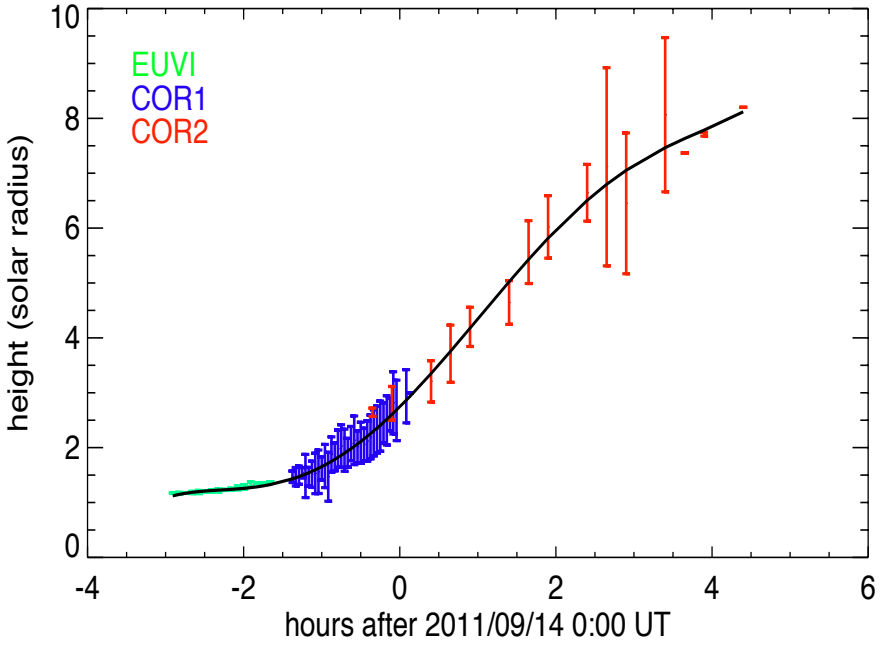

height, velocity, and acceleration of CMEs

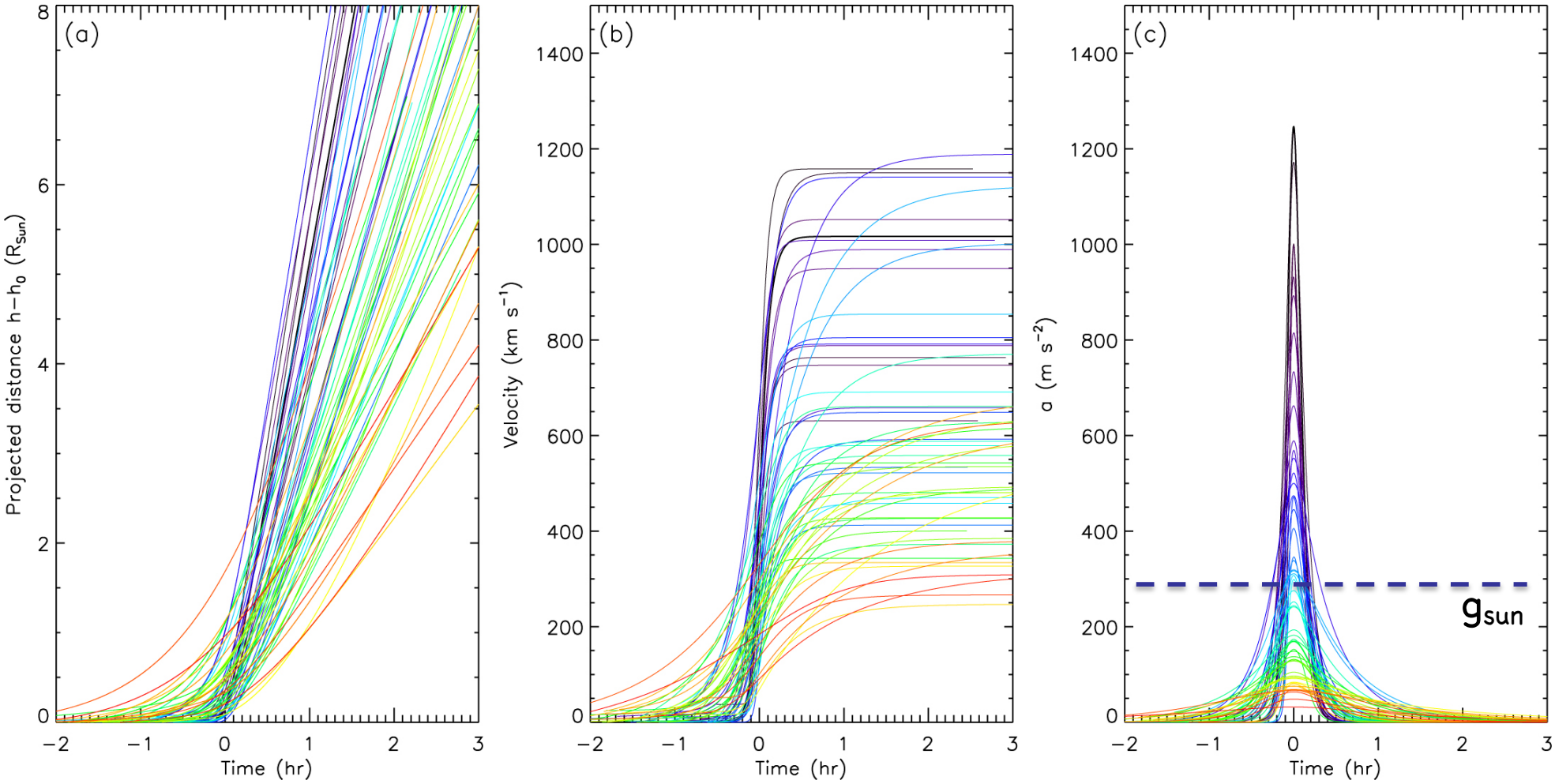

Fast CMEs are accelerated within minutes in the low corona (Zhu et al. 2020).

mass and energy of CMEs

$$E = \frac{1}{2}Mv^2 + \frac{1}{2}Mv_{esc}^2\left(1 - \frac{R_s}{R}\right) + \frac{M}{m}kT$$

CME mass is estimated from the white-light images, where enhanced brightness is due to Thomson scattering by electrons (Vourlidas et al. 2000, 2006), ranging from 10^{13-16} grams.

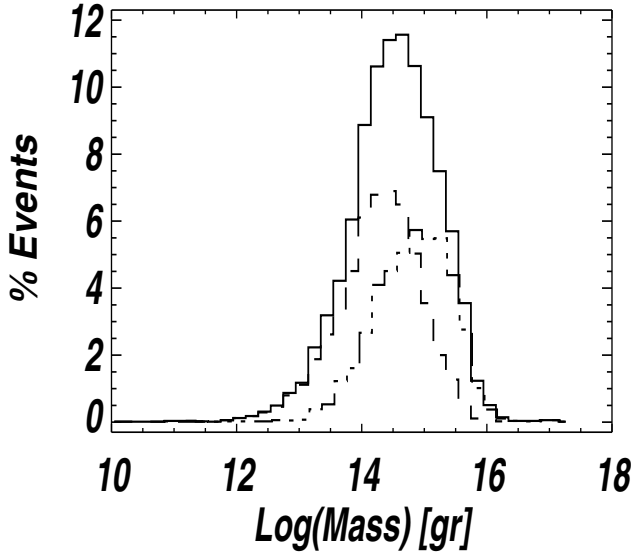

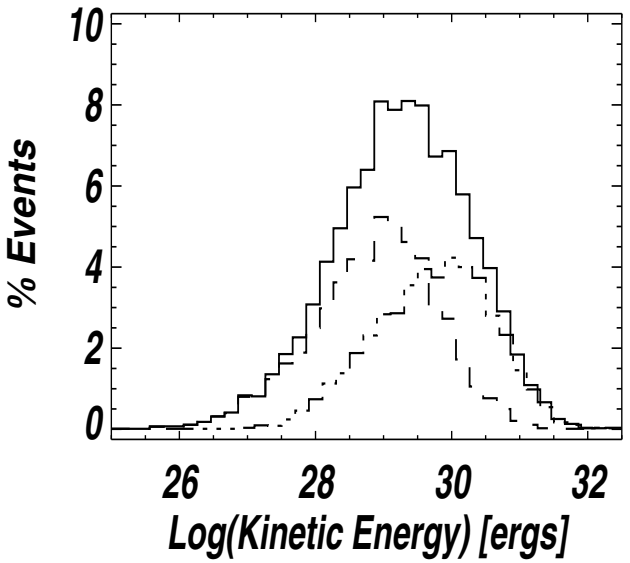

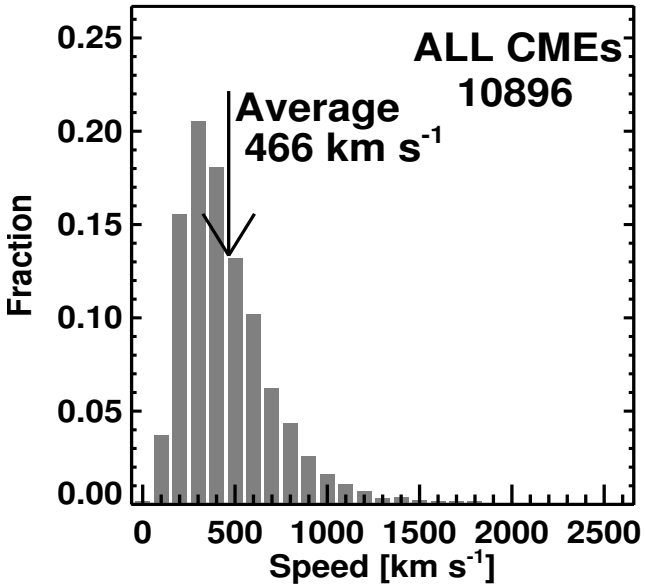

Vourlidas et al.

Gopalswamy, Yashiro at al.

CME properties inferred from coronal dimming

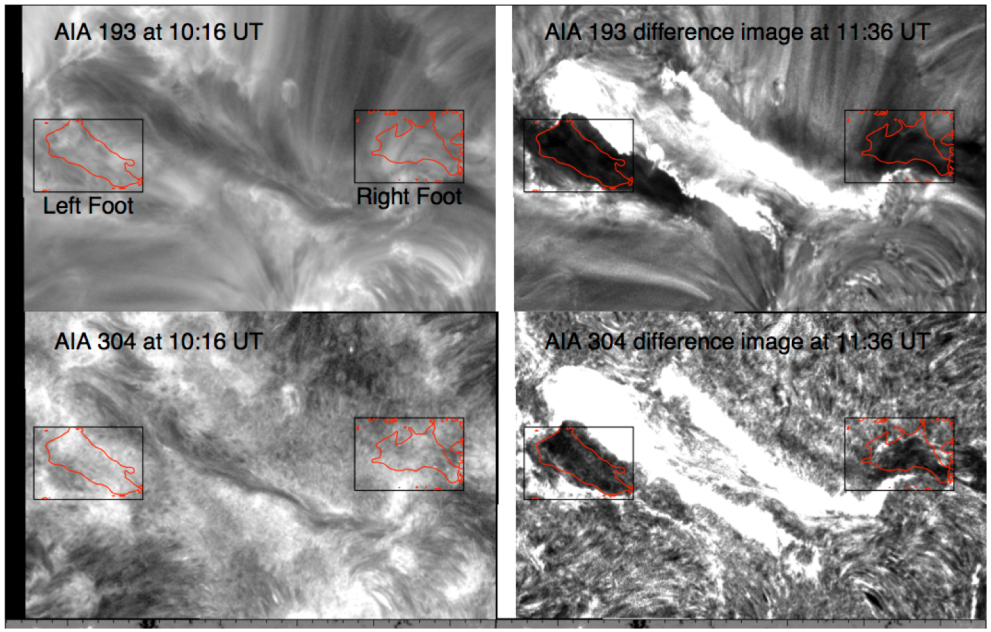

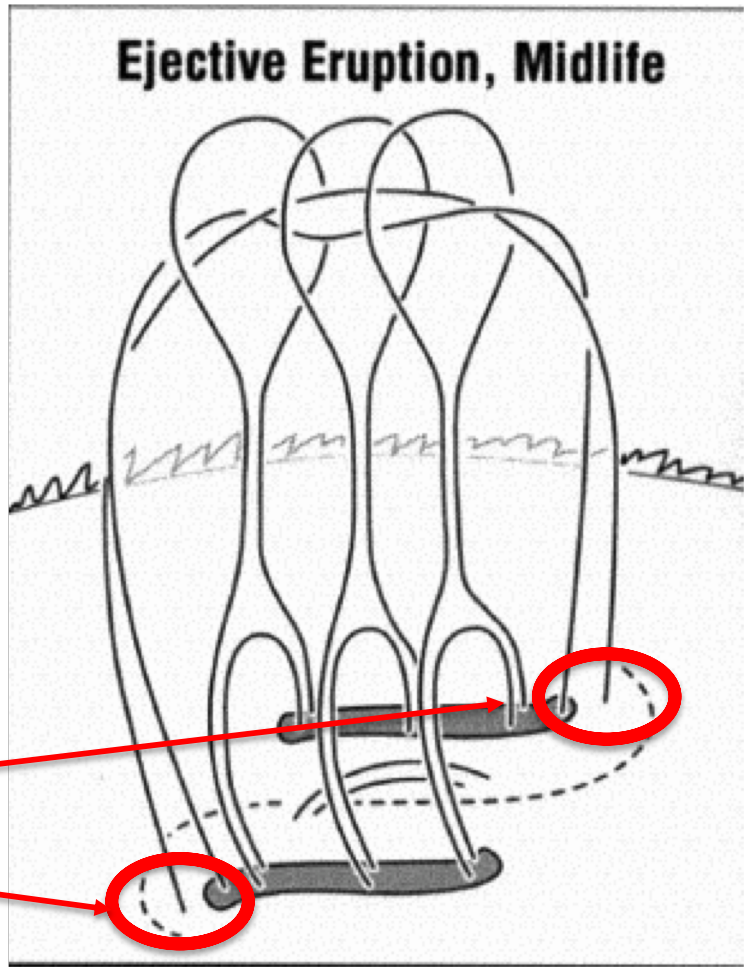

The erupting rope causes coronal dimming at the two feet, with which the axial flux of the rope is estimated.

Moore et al. (2001)

CME kinematics inferred from coronal dimming

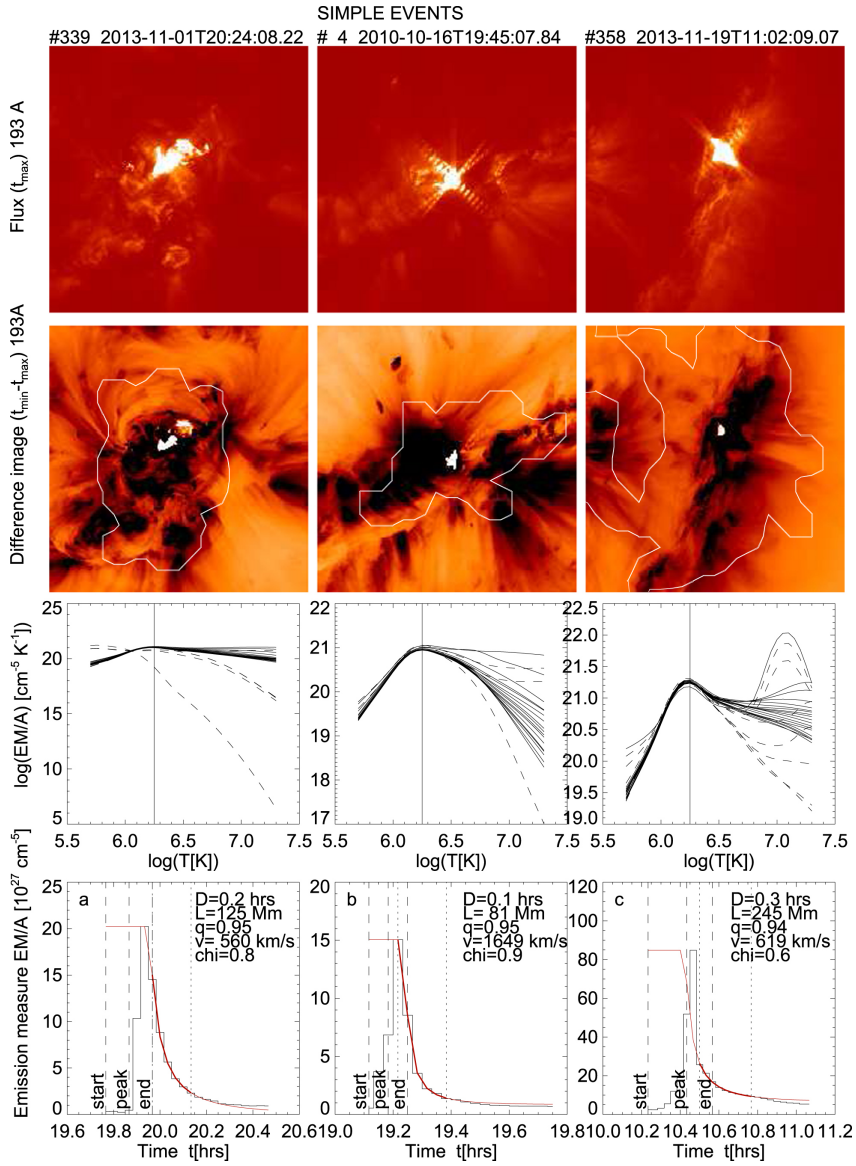

Aschwanden 2016

As CME expands, the emission measure (EM) decreases, and the corona becomes dimmer.

$$EM = \int n^2 dl$$

$$= \int \boxed{n^2 \frac{dl}{dT}} dT$$

DEM

$$I \sim \int \boxed{n^2 \frac{dl}{dT}} G(T) dT$$

$$\ln\left[\frac{I(t)}{I(t_0)}\right] \sim -\alpha \ln\left[\frac{H(t)}{H(t_0)}\right]$$

energies of CMEs, flares, and magnetic fields

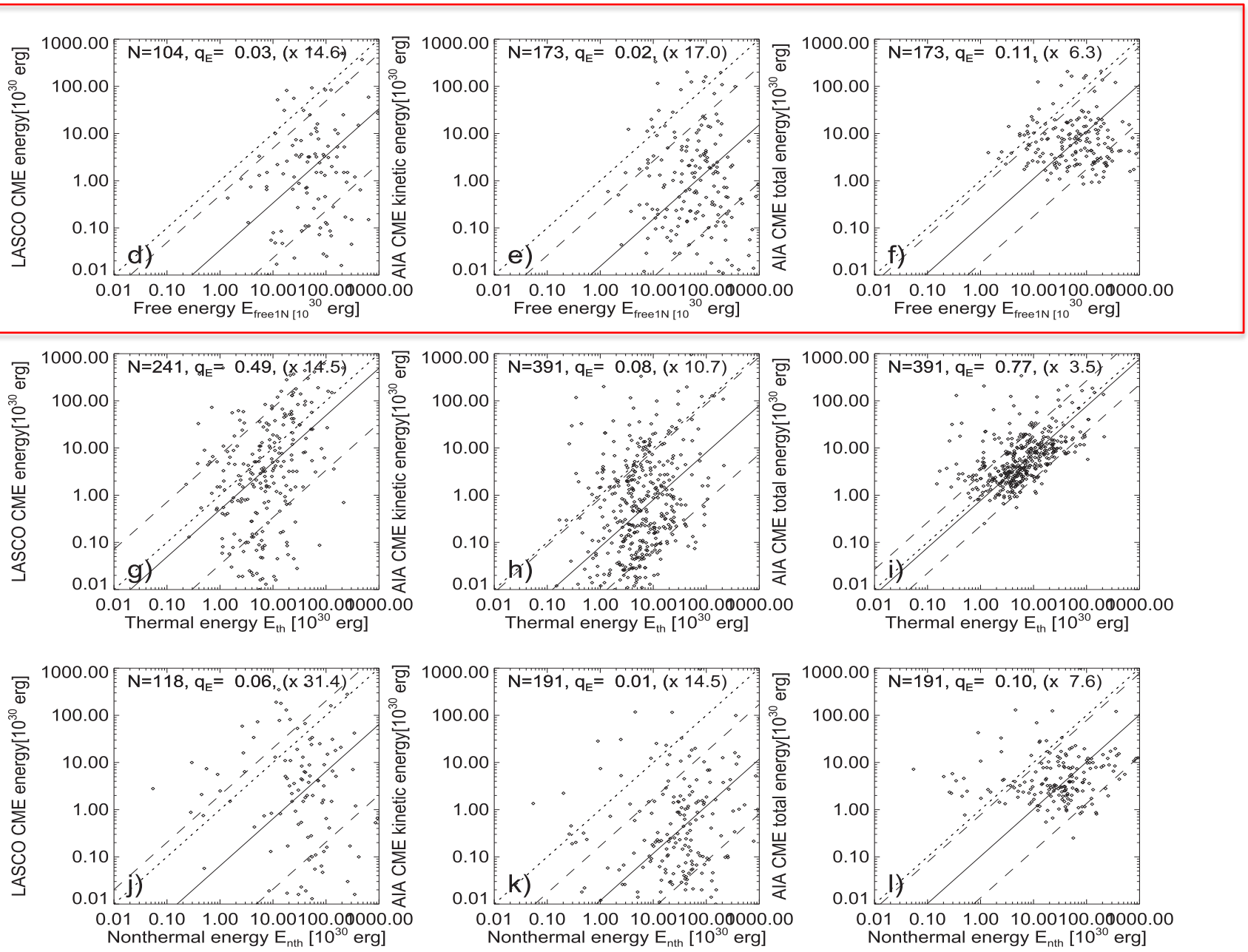

how to predict eruptions?

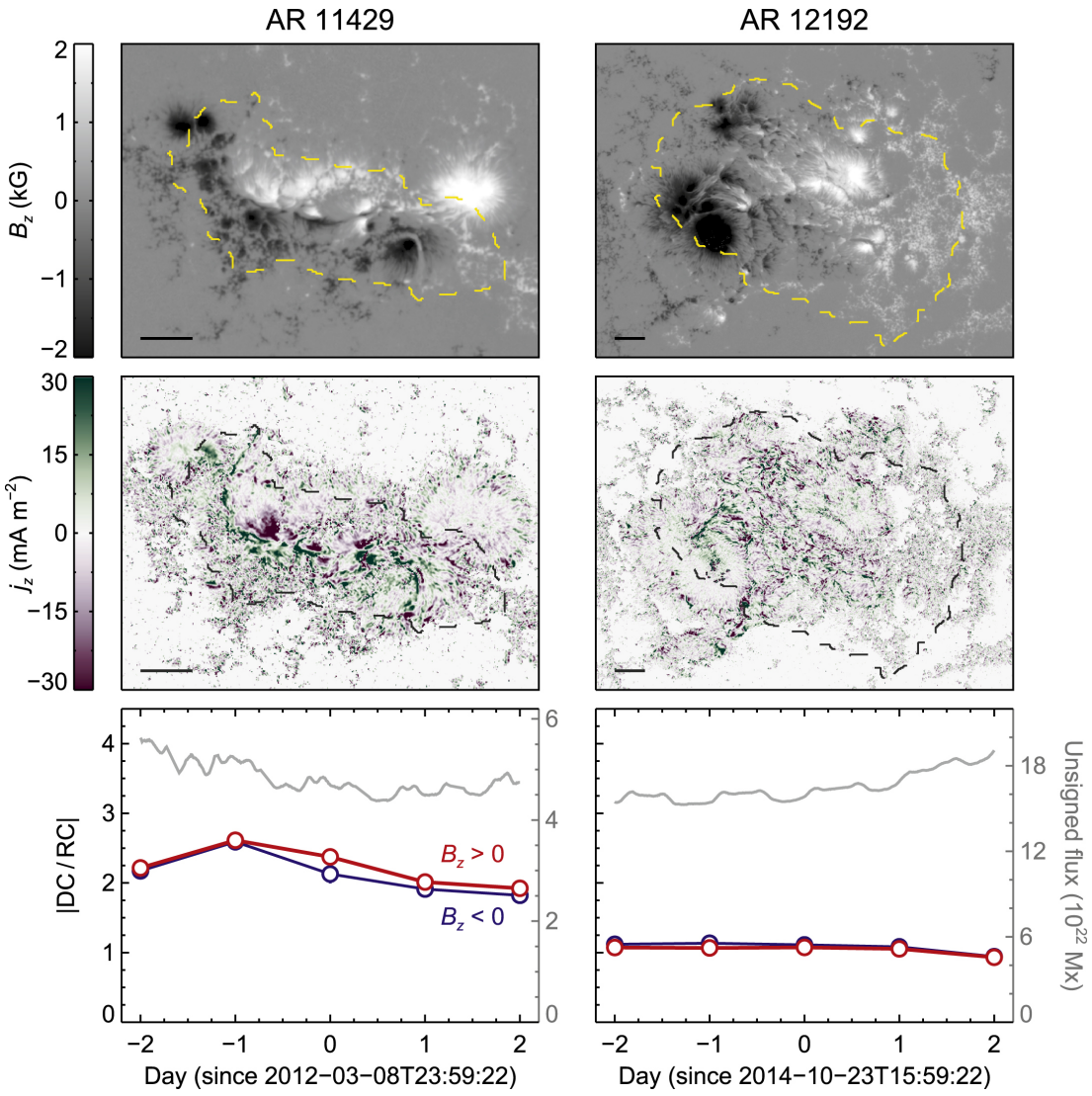

Liu et al. 2017

Searching for **non-potential** magnetic parameters to predict eruptions is still underway (Schrijver 2007, Falconer et al. 2009, Barnes et al. 2016, Sun et al. 2015, Liu et al. 2017, Cui et al. 2018, Green et al. 2018).

Numerical models are starting to tackle real active regions and provide physics diagnostics (Van Ballegooijen et al. 2004-, Torok et al. 2004-, Fan et al. 2005-, Aulanier et al. 2010-, Jiang et al. 2012-, …. Karpen et al. 2012).

Summary notes

Observations by a cohort of telescopes with multi-spectral capabilities as well as multiple view points have significantly advanced our knowledge of the structure, properties, and evolution of CMEs.

Numerical models are challenged by as well as taking advantage of emerging observational details of CMEs and ambient magnetic fields. The combined model-observation effort will help improve understanding of mechanisms driving solar eruptions that impact space weather.